

Citation for the published version:

Al-Tabbaa, A., Litina, C., Giannaros, P., Kanellopoulos, A., & Souza, L. (2019). First UK field application and performance of microcapsule-based self-healing concrete. *Construction and Building Materials*, 208, 669-685. DOI: 10.1016/j.conbuildmat.2019.02.178

Document Version: Accepted Version

This manuscript is made available under the CC-BY-NC-ND license
<https://creativecommons.org/licenses/by-nc-nd/4.0/>

Link to the final published version available at the publisher:

<https://doi.org/10.1016/j.conbuildmat.2019.02.178>

General rights

Copyright© and Moral Rights for the publications made accessible on this site are retained by the individual authors and/or other copyright owners.

Please check the manuscript for details of any other licences that may have been applied and it is a condition of accessing publications that users recognise and abide by the legal requirements associated with these rights. You may not engage in further distribution of the material for any profitmaking activities or any commercial gain. You may freely distribute both the url (<http://uhra.herts.ac.uk/>) and the content of this paper for research or private study, educational, or not-for-profit purposes without prior permission or charge.

Take down policy

If you believe that this document breaches copyright please contact us providing details, any such items will be temporarily removed from the repository pending investigation.

Enquiries

Please contact University of Hertfordshire Research & Scholarly Communications for any enquiries at rsc@herts.ac.uk

5 First UK field application and performance of 6 microcapsule-based self-healing concrete 7

8 Abir Al-Tabbaa^a, [Chrysoula Litina](#)^{*a}, Petros Giannaros^{a1}, Antonios Kanellopoulos^{a2} and Livia
9 Souza^a
10

11 ^aDepartment of Engineering, University of Cambridge, Trumpington Road, Cambridge CB2 1PZ, UK
12

13 *Corresponding authors:

14 Chrysoula Litina, cl519@cam.ac.uk, Department of Engineering, University of Cambridge,
15 Trumpington Road, Cambridge CB2 1PZ, UK
16
17

18 Abstract

19 Maintaining the health and reliability of our infrastructure is of strategic importance. The current state
20 of the UK infrastructure, and the associated huge costs of inspection, maintenance, repair and
21 eventual replacement, is not sustainable and is no longer environmentally viable. The design of
22 infrastructure, mainly concrete, remains traditional and poor material performance continues to be
23 the main cause of deterioration and failure in our infrastructure systems. Biomimetic materials, that
24 emulate natural biological systems in their ability to self-healing, provide an exciting and plausible
25 solution. Embedding cementitious materials with in-built capabilities to sense and respond to their
26 environmental triggers could potentially eliminate all external interventions and deliver a resilience
27 infrastructure. The work presented in this paper forms part of a national initiative that has been
28 developing biomimetic cementitious infrastructure materials which culminated in the first large-scale
29 field trials of self-healing concrete in the UK testing four different but complementary technologies
30 that were developed. This paper focuses on one self-healing technology, namely microcapsules, which
31 contain a healing agent that is released on their rupture as a result of crack propagation. The paper
32 will present details of the microcapsules used, their implementation in concrete and in the field trials
33 and time-related, field and laboratory, assessment of the self-healing process. It also highlights
34 challenges faced and improvements that are now on-going to produce the next generation of the
35 microcapsule self-healing cementitious system.
36

37 Keywords

38 Self-healing, concrete, site trials, materials for life. microcapsules, applications, construction,
39 materials, testing

¹ Present address: Klohn Crippen Berger, Vancouver, BC, V5M 4X6, Canada

² Present address: School of Engineering and Technology, University of Hertfordshire, College Lane Campus,
Hatfield, AL10 9AB, UK

40 1 Introduction

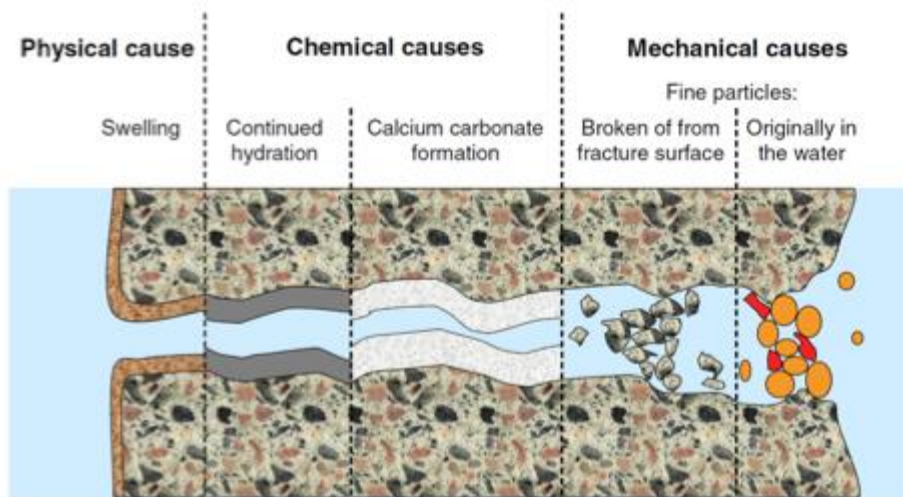
41 1.1 Infrastructure and biomimetic materials

42 Infrastructure assets (e.g. bridges, tunnels, motorways, dams and embankment) are a nation's lifeline
43 and are vital for societal and economic growth. The deteriorating state of the ageing UK infrastructure,
44 and similarly around the world, is the result of decades of underinvestment. The UK recently
45 committed to an investment of £500 Billion in infrastructure by 2020-2021 [1] in valiant efforts to save
46 the nation's infrastructure assets. The majority of infrastructure assets are made out of cementitious
47 composites, mainly concrete. Current figures show that half of the construction budget is spent on
48 the repair and maintenance of mainly concrete infrastructure at around £40 Billion/year [2]. Concrete
49 deterioration is the result of traditional civil engineering design practices that are still based on the
50 assignment of appropriate partial material and action factors and providing redundancy to prevent
51 failure. Material degradation is viewed as inevitable and mitigation necessitates expensive inspection,
52 maintenance, repair and replacement regimes. Hence poor material performance continues to be the
53 single main cause of deterioration and failure in our infrastructure systems. Moreover, the durability
54 of repaired concrete structures continues to be major concern as after 5 years, 20% of all repairs fail,
55 increasing to 55% after 10 years [3].

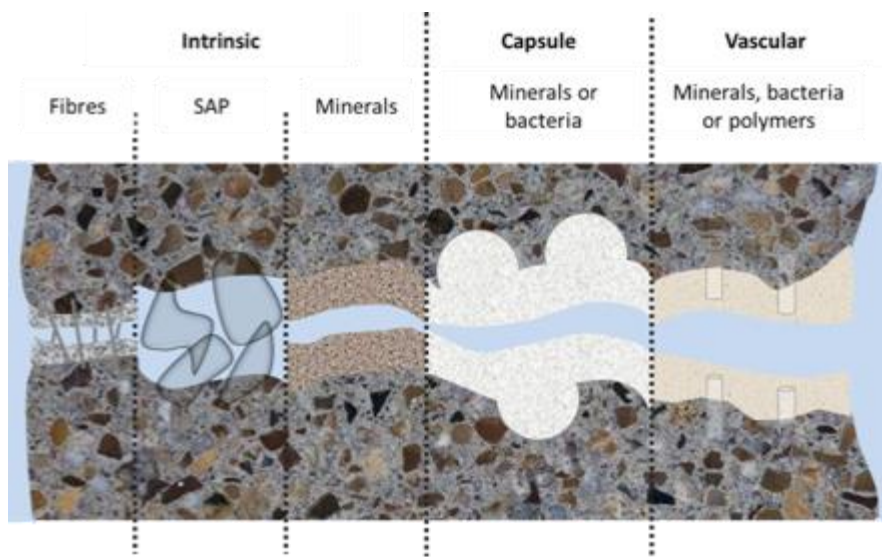
56 While the construction industry is the single largest consumer of resources and raw materials, and
57 accounting for 6% of GDP, it remains the slowest sector to adopt and adapt to new technologies and
58 advanced materials, due to its historic conservative approach to product design and delivery [4].
59 Construction materials have historically suffered from being perceived fundamentally as a cheap and
60 straightforward commodity, where the application of often expensive cutting-edge material
61 technologies is simply not justified. This view can no longer be sustained due to the huge volumes
62 used and associated high carbon footprint as well as the extensive and expensive maintenance
63 regimes that are needed to maintain our infrastructure assets. A new approach to material design
64 through mimicking natural biological systems, in their ability to self-heal, has been adopted in some
65 sectors, with commercial success, through the development of a new class of biomimetic materials.
66 Biomimetic materials are advanced materials that can transform our infrastructure by embedding
67 resilience within its components and systems so that rather than being defined by individual events,
68 they can evolve and adapt over their life span. National and international government and industry
69 road-mapping reports [4–7] have highlighted that advanced infrastructure materials, with specific
70 reference to biomimetic attributes, will play an essential part in the future transition of infrastructure.
71 This will provide a much higher level of confidence in the reliability of the performance of our
72 infrastructure systems but will also require a complete paradigm shift across the design, procurement,
73 construction and maintenance of our infrastructure.

74 In cementitious systems, while different forms of damage result from the wide range of environmental
75 and mechanical actions, cracking is the most widely and commonly encountered. As a result self-
76 healing of cracks in cementitious systems has been widely studied [8,9]. In this context, self-healing
77 phenomena in cementitious systems are broadly classed into two categories: Autogenic and
78 Autonomic (Fig. 1a-b). Autogenic self-healing refers to self-healing processes that are an intrinsic
79 characteristic of the components of the matrix which are usually effective for small crack widths of
80 $\leq 0.15\text{mm}$ and under water curing. Autonomic self-healing refers to actions that use components that
81 do not naturally exist in the cementitious composite, i.e. 'engineered' additions that are usually
82 employed to deal with larger crack sizes and under less favourable curing environments. Some
83 autogenic and autonomic self-healing systems work in combination so that the autonomic system
84 works to reduce the crack size to enable autogenic processes to complete the self-healing process.
85 The work presented in this paper relates to the use of microcapsules for autonomic self-healing in
86 cementitious systems.

87



(a)



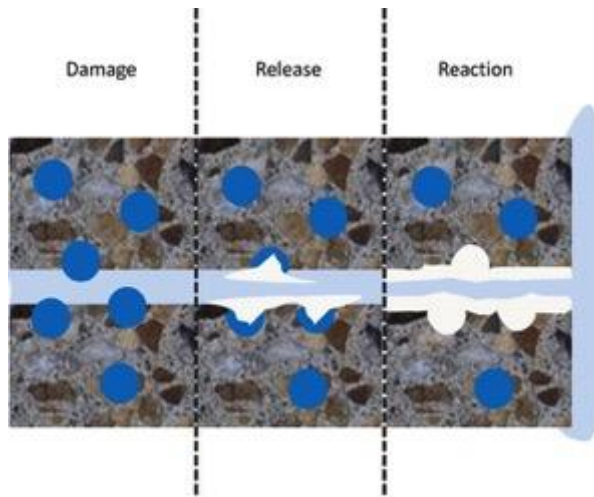
(b)

Figure 1 Self-healing mechanisms for cracks in cementitious systems (a) autogenic self-healing (Reproduced with permission, 2013 Springer [8]) and (b) autonomic self-healing (Reproduced with permission [10]).

1.2 Microcapsule-based systems for self-healing in cementitious systems

Microcapsules are micron-size particles consisting of a stable shell enveloping a cargo, which could be solid, liquid or gases, and serve a wide range of applications in different sectors. They are already in commercial use in construction materials for heat proofing, e.g. phase change materials, and air entraining agents, both incorporated directly into the building material mix composition [11]. Since White et al. [12] introduced the use of microencapsulation for self-healing of polymers in 2001, microencapsulated healing agents for autonomic self-healing has attracted much attention. Embedded microcapsules in materials imbue the ability of a localised response to damage upon rupture, and subsequent release and activation of the healing agent. The proof of concept for microcapsule-based healing in concrete was recently demonstrated [13,14]. The fundamental principle of autonomic self-healing via microencapsulation is that when cracks propagate in the cementitious matrix, they mechanically rupture the dispersed microcapsules and their content (cargo material) is released into the crack volume. Similar to encapsulation, the self-healing mechanism will rely on the nature of the cargo material; namely it may react with an activator (provided as a two-part system e.g. 2-part epoxy system), the cementitious matrix (including hydration and carbonation

112 products e.g. lime) or the environment (e.g. air, moisture for example cyanoacrylates) to form
113 products that fill, seal or heal the crack (Fig. 2). Much of the published literature on
114 microencapsulation-mediated healing has focused on cyanoacrylates or 2-part epoxy for their rapid
115 hardening and high strength, hence quickly providing strength regain. However their high toxicity,
116 high cost and short shelf-life prohibit their use commercially. Recent research has focused on the
117 development of suitable microcapsules taking into consideration parameters affecting the bond
118 strength and boundary conditions to enhance chemical compatibility with the cementitious matrix.
119 Moreover healing agents that can deliver healing products of more compatible nature to the concrete
120 matrix such as encapsulated bacterial spores and mineral cargos including colloidal silica and sodium
121 silicate have recently been considered. A review of the various microcapsules systems can be found
122 elsewhere [9].



123

124 **Figure 2 Schematic of microcapsule mediated self-healing in concrete [10].**

125 A number of experimental procedures have been developed and used to assess the self-healing
126 efficiency in cementitious systems which include quantification of the mechanical recovery (e.g.
127 compressive and flexural strength) using multiple cycles of static loading and reloading or non-
128 destructive measurements as well as permeability measurements [15]. A review of the recent
129 literature, relevant to self-healing microcapsules, shows changes in a variety of material properties
130 when adding microcapsules into cementitious mixes; including workability, permeability, elasticity
131 and strength, although the exact effect is highly dependent on the dosage, size, cargo and particular
132 characteristics of the microcapsules [9].

133 Previous work by the authors confirmed the potential of mineral microencapsulated cargos, in glass
134 tubes, for use in self-healing cementitious materials, with a focus on sodium silicate [16,17] which is
135 commonly used as a repair agent. Different polymeric microencapsulation systems for the sodium
136 silicate were considered [10,18]. The most promising developments included the production of
137 microcapsules with polymeric gelatin/gum Arabic shell, with switchable mechanical properties that
138 ensured the required performance during the mixing and in response to a mechanical trigger [19]. The
139 effect of these sodium silicate containing microcapsules was investigated on both the fresh (viscosity,
140 setting time) and hardened properties (modulus of elasticity, compressive and flexural strengths) [19–
141 21]. In these studies, work was also carried out on identifying the healing potential of these
142 microcapsule-based systems under different cracking regimes and degrees of damage. While mineral
143 healing agents do not provide the same level of mechanical strength recovery as its cyanoacrylate
144 counterparts do, they were show to provide significant permeability reduction, hence providing
145 efficient sealing and healing that will prevent ingress of aggressive chemicals and protect against
146 corrosion.

1.3 Large-scale and field application of self-healing concrete

147
148 To date, most of the developments on autonomic self-healing cementitious systems have largely taken
149 place in the laboratory. The first scale-up application of self-healing technologies in concrete was
150 carried out in the 1990s by Dry at the University of Michigan simulated different damage scenarios for
151 bridge elements and pavements in full scale and later field scale trials [22]. Reinforced concrete beams
152 (0.15m x 0.15m x 1.8m) were constructed with embedded continuous brittle glass tubes in their
153 tensile side. Three different healing agents were investigated including a two-part epoxy,
154 cyanoacrylate and a silicon-based adhesive. The reinforced concrete beams were cracked to failure
155 under three-point bending, allowed to recover and then retested to assess the potential for
156 mechanical recovery. Although the reported results were inconsistent as to the performance of the
157 healing technology, some strength regain was possible. Since then, other scale-up work of reinforced
158 concrete samples with embedded glass tubes containing self-healing agents and subjected to cycles
159 of loading and unloading was reported. Thao [23] considered a series of reinforced concrete elements
160 embedded with glass tubes containing an isocyanate prepolymer fastened to their reinforcement
161 bars. A concrete beam (125mm x 200mm x 2000mm), concrete columns (200 x 800mm) and slabs
162 (1000mm x 10000mm x 100mm) were investigated. When the beam was loaded under four-point
163 bending, the embedded tubes showed breakage and subsequent release of the encapsulated agent.
164 Columns were loaded to induce cracking and release of healing agents. Reloading of the column
165 showed the formation of new cracks without any reopening of the previously healed cracks, due to
166 complete recovery of the strength following self-healing. Subjected to impact-loading, the control slab
167 showed a continuous loss in stiffness whilst the self-healing slab showed stiffness recovery up to 99%.
168 Similarly Karaiskos et al [24] also added glass-encapsulated healing agents (polyurethane) into a
169 150mm x 250mm x 3000mm reinforced concrete beam. 350 glass tubes each 50mm in length were
170 added 10mm from the base of the beam by attaching them to a plastic grid. Cracks were induced by
171 loading the beam in four-point bending until the average measured crack width reached 0.25mm.
172 Beams were then reloaded after a seven-week healing period and several non-destructive testing
173 (NDT) methods were used to monitor healing of cracks. These included ultrasonic pulse velocity,
174 piezoelectric transducers, acoustic emission and digital image correlation. Results were compared
175 with a control beam without the glass tubes. No significant recovery in mechanical properties was
176 observed for either beam although the use of a variety of NDT methods proved useful for monitoring
177 crack formation, propagation and closure.

178 Transfer of developed self-healing technologies from larger laboratory-scale experiments to field-
179 scale structures has been limited. In addition to overcoming practical challenges of up-scaling the
180 healing technology, the in-situ application of any self-healing approach possesses unique challenges
181 and obstacles. Field scale reinforced concrete applications of capsule-based self-healing concrete have
182 been implemented [25,26]. Full scale reinforced concrete bridge decks (7m x 1.2m x 0.075m) were
183 constructed, embedded with discrete glass fibres (100 μ m) containing a combination of
184 sealant/adhesives. Brittle fibres placed close to the surface of the bridge deck targeted transverse
185 shrinkage cracking. After one month, the fibres were seen to break releasing the sealant creating a
186 controlled expansive joint. The efficiency of the healing mechanism under mechanical damage was
187 also investigated. Load-induced cracks were generated using a pneumatic jack at mid-span causing
188 the glass fibres to break and release the adhesive into the cracks. Subsequent reloading of the bridge
189 deck was also conducted to test the efficiency of the adhesive in the regain of mechanical
190 performance. Increased strength regain was demonstrated compared to a control deck with new
191 cracks opening during reloading before the original cracks reopened. Re-release of repair adhesives in
192 second and third loadings occurred in all of the decks containing repair adhesives showing good long-
193 term survivability of the encapsulated healing agent. A few large scale field applications of bacteria-
194 based self-healing concrete have also been realised [27,28]. Here, bacteria were added into the
195 concrete mix that metabolise added calcium lactate to produce calcium carbonate. The first field
196 application involved 3m-long concrete linings for an irrigation canal in Equador containing LWAs
197 impregnated with alkaliphilic spore-forming bacteria [29]. After five months, the cast concrete showed

198 no sign of cracking or deterioration and therefore its healing performance could not be evaluated.
199 Researchers at Delft University of Technology were first to implement self-healing concrete in a
200 building[28]. A lifeguard station consisting of bacteria-based concrete has also been built [30].
201 However, no publication of results of how the building is performing to date could be obtained.

202 A national UK team, from the universities of Cambridge, Cardiff and Bath, has come together, through
203 research council funding, to develop the first generation of self-healing cementitious systems in the
204 UK to address cracks across many length scales [31–33]. This led to the development of a suit of
205 complementary technologies namely microcapsules, calcite precipitation bacteria, shape memory
206 polymer tendons and vascular networks (Fig 1b). These can be used in isolation or in combination
207 depending on the nature and extent of the damage. Extensive system development and material
208 testing was carried out in the laboratory. Collaboration with industry partners led to scaling up of the
209 technologies and to the first UK full-scale field trials of the developed system in concrete retaining
210 wall panels, on the Welsh Government A465 Heads of the Valleys Upgrade scheme project. Five
211 concrete panels were cast- each being 1.8m tall, 1m wide and 150mm thick (shown in Fig. 3). Details
212 of the design and execution of the field trials were presented elsewhere [34,35]. One of the panels
213 contained the developed microcapsules and there was a control panel without any microcapsules with
214 which a comparison was made. This paper focuses on the former. It presents details of the scaling up of
215 the microcapsules and their use in the field trials and subsequent performance and monitoring.



216
217 **Figure 3 Self-healing concrete wall panels constructed within the EPSRC and industry funded**
218 **Materials for Life (M4L) project [35].**

219 2 Materials and Testing

220 2.1 Microcapsules and concrete mixes

221 The microcapsules used here were the result of industrial collaboration, which led to the design and
222 production, using complex coacervation, of gelatin/gum Arabic shell microcapsules containing
223 sodium silicate (SS) as the cargo [19]. The sodium silicate was in an emulsion with mineral oil and
224 emulsifier and formed ~42% of the cargo. The microcapsules (seen in Fig. 4a) had a mean diameter of
225 290 μm with a standard deviation of ~120 μm and were provided in a preserving solution (Fig. 4b). The
226 microcapsules had switchable mechanical properties such that they initially had ductile ‘rubbery’
227 behaviour, which guaranteed their survivability during concrete mixing, and then became brittle, and
228 easy to fracture, in the set concrete as water was removed from the shell [19]. Based on the results
229 from related laboratory studies on the effect of the microcapsules on the fresh and hardened material
230 properties and healing potential of mortars [21] and concrete [36], 8% microcapsule content by
231 volume of cement (v_c) was selected for application in the field trials. This dosage was found to provide
232 an optimum level of healing, showed high compatibility with the mortar matrix and had negligible
233 effects on the workability, setting time and strength development.

234 The concrete mix composition is detailed in Table 1. The microcapsules were first washed with water
 235 and filtered from their preserving solution before being added, in their slurry form, directly into the
 236 ready-mix C40/50 concrete using a portable 120L Belle concrete mixer. The microcapsules were added
 237 at 8% by volume of the cement, corresponding to $\sim 2.67\%$ by weight of the cement and $\sim 0.47\%$ of the
 238 total concrete mix. A small quantity of water was used to wash out the microcapsules from the
 239 container and as a result the effective water-to-cement (w/c) ratio of the concrete mix increased from
 240 ~ 0.43 to ~ 0.45 . A control panel was also cast without any microcapsules.



241 (a)

242 (b)

243 **Figure 4** The microcapsules used in the field trials; (a) the microcapsules under the microscope [19]
 244 and (b) microcapsule slurry as delivered to site [35].
 245

246

247 **Table 1** Composition by % weight of the ready mix C40/50 concrete (supplied by Hanson UK) and
 248 the microcapsules used in the site trial.

Material	Quantity for field trials (kg/m ³ unless noted otherwise)
Cement (CEM I)	415
10mm Limestone aggregates	944
Limestone fines (0-2mm)	396
Marine sand	393
Water	179 (w/c 0.43)
Admix: Plasticiser	0.35 L/100kg cement
Admix: Retarder	0.1 L/100kg cement
Microcapsules (slurry)	11.1

249

250 2.2 Crack initiation and monitoring

251 The wall panels were designed to crack 500mm from the base upon loading, which was facilitated by
 252 using 16mm diameter starter bars on the front face up to the designed crack location, before changing
 253 to the 10mm diameter mesh to create a weak section in the panel as seen in Fig. 5. Loading was
 254 applied using a hydraulic jack positioned 1.5m above the base of the panels, i.e. near the top of the
 255 wall, that was used to pull a threaded bar; thereby inducing a cantilever load. A wailing beam attached
 256 to the front of the panel allowed a distribution of load across the width of the wall. Full details of the
 257 design and construction of the walls is given elsewhere [35]. Panels were painted with a black-and-
 258 white speckle pattern for digital image correlation (DIC) analysis to monitor wall displacements and
 259 associated strains that arise during loading and unloading (Fig. 6).

260 Prior to loading, air permeability measurements at various locations around the wall face were taken
 261 as initial reference measurements using a field permeability tester [37], particularly in the region
 262 where cracking was expected to occur (Fig. 7). The permeability of the concrete cover (that between
 263 the steel reinforcement and external environment) must be sufficiently sound as an indicator of good

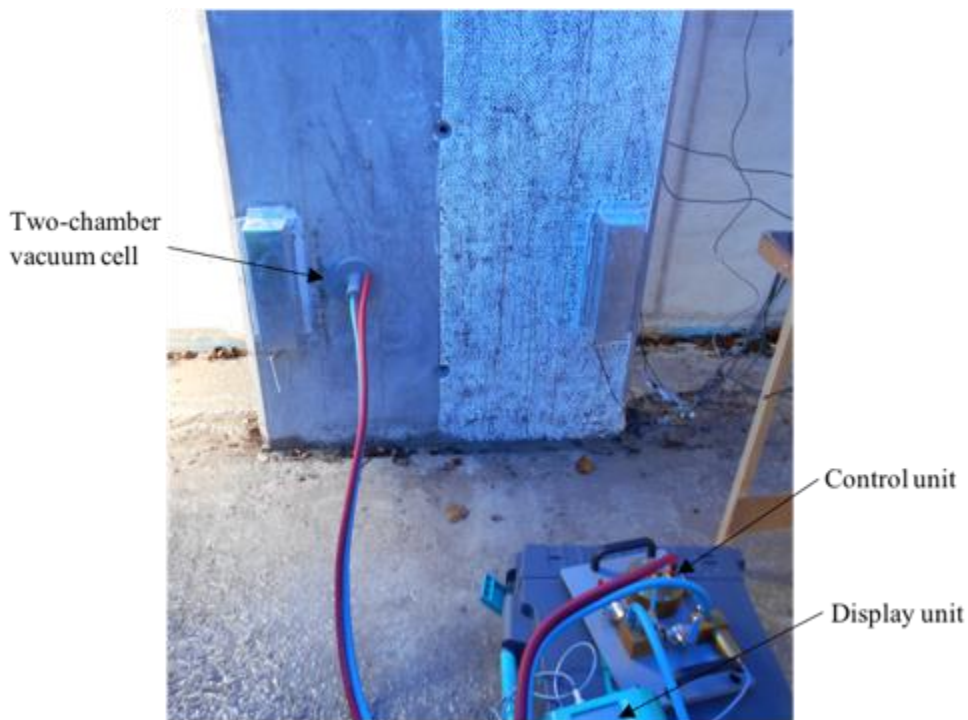
264 durability. Air permeability testing allows a non-destructive measurement of the quality of the
265 concrete cover on site and involves applying a vacuum inside a cell placed on the concrete surface and
266 then measuring the rate at which the pressure returns to the atmospheric value. The two-chamber
267 vacuum cell is connected to a pressure regulator that balances the pressure in the inner (measuring)
268 chamber and in the outer (guard-ring) chamber. Data was collected automatically by the display unit
269 and the permeability coefficient (kT) and the depth of penetration (L) of the vacuum was calculated.
270 The air permeability measurements are generally in good agreement with laboratory methods [37]
271 and the testing equipment adheres to SN 505 252/1, Annex E.



272
273 **Figure 5 Wall panel reinforcement design to ensure cracking at ~500mm from the base of the wall**
274 **panel.**



275
 276 **Figure 6 The microcapsule wall panel half painted with a black-and-white speckle pattern for DIC**
 277 **analysis**

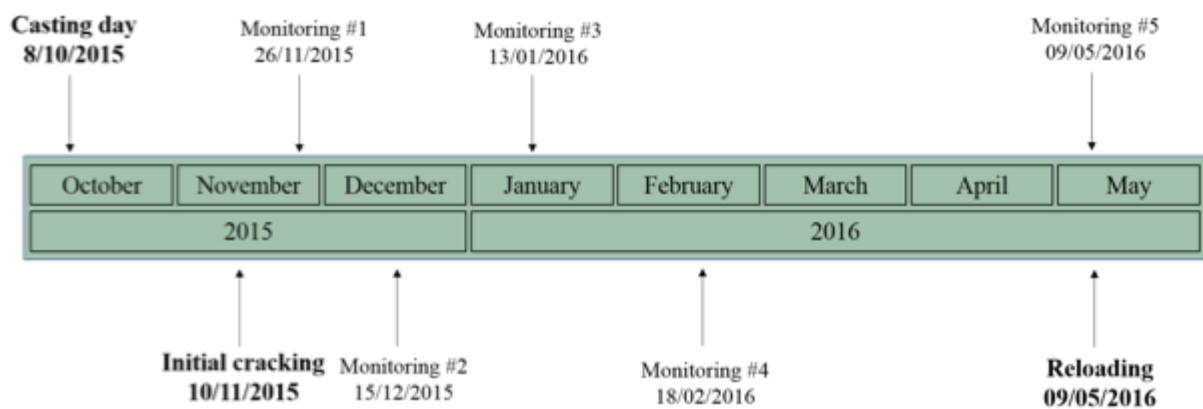


278
 279 **Figure 7 Air-permeability testing device obtaining measurements around the expected crack**
 280 **generation area.**

281

282 A timeline of the field trials experimental programme is given in Fig. 8. The wall panels were initially
 283 loaded 5 weeks after their casting day and then reloaded after a 26-week healing period. Loading was
 284 applied until a noticeable crack appeared at the designed height and a large drop-off in load was

285 observed. After the healing and monitoring period, the walls were reloaded to the residual (drop-off)
 286 load. Four linear variable differential transformers (LVDTs) were used to measure lateral wall
 287 displacements. The LVDTs were located at the same height as the load application: two recording
 288 displacements of the wall panel and two recording displacements of the reaction wall. A mean of the
 289 lateral wall displacement was used when plotting load-displacement curves. A further two LVDTs were
 290 used to record crack opening by mounting them vertically on the front of the wall panel, ensuring that
 291 they span across the expected location of induced crack. Demountable mechanical strain gauge
 292 (DEMEC) pips were attached adjacent to the LVDTs to measure crack opening (Fig. 9). Once the panels
 293 were cracked, the load was kept constant and DEMEC measurements were taken. To complement the
 294 latter, microscope images were taken along the crack length spanning the panel width using a
 295 handheld digital microscope. After the acquisition of DEMEC measurements and microscope images,
 296 the load was gradually released from the wall panel. After complete unloading, DEMEC measurements
 297 and microscope images were taken once again, at the same exact points, to measure the residual
 298 crack width.



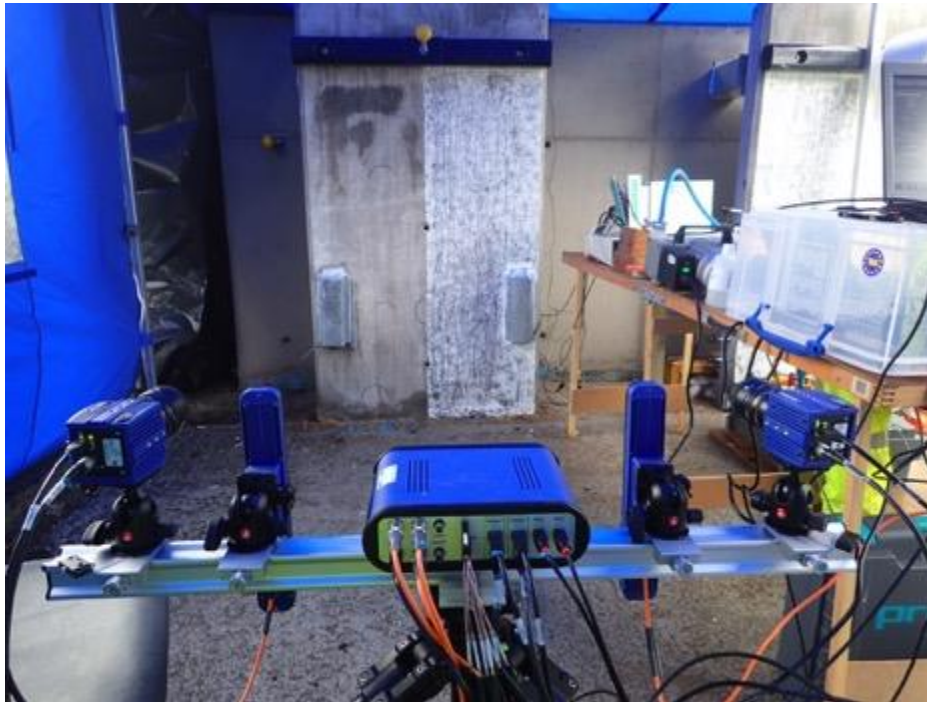
299 **Figure 8 Timeline of wall panels testing and measurement collection dates**
 300



301 **Figure 9 Location of DEMEC pips, ultrasonic probe measurement locations and air permeability**
 302 **measurement locations.**
 303

304
 305 The DIC software measured displacements through the comparison of images to monitor movement
 306 in the speckle pattern. Photographs of the wall were taken at each kN load applied (or released) using
 307 two digital cameras and flash equipment set up on a tripod facing the wall panel (Fig. 10). The use of
 308 DIC allowed monitoring of crack initiation, coalescence and propagation. The covering of one-half of
 309 the wall face only in the speckle pattern offset any potential variations in obtained measurements due
 310 to the hydrophobic/water repellent nature of the paint. After initial cracking, a strip of thermal
 311 insulation foil roll was placed across the middle section the microcapsule wall to reduce its exposure
 312 to the environment. This was to examine the effect of sealing on the overall healing progress for both
 313 halves of the wall although the insulation was permanently removed after Monitoring event #1.

314 Weather data was collected from local weather stations in Tredgar and Usk between October 2015
315 and May 2016 including daily minimum air temperature, maximum air temperature and total rainfall.



316
317 **Figure 10 Digital Image Correlation camera and tripod set-up on the microcapsule wall.**

318

319 Between initial cracking and reloading stages, various measurements were periodically taken from the
320 wall panels to assess crack closure and monitor self-healing. Microscope images were taken from at
321 least five observation locations along the crack length. Using this data, interpolation of crack width
322 along the crack length was carried out allowing a visual representation of crack width across the wall
323 panel throughout the healing period. Crack width healing values were also calculated in order to
324 quantify crack closure. The crack width healing percentage compares measured crack width values
325 with the initial crack opening at that point following cracking and load-release. Crack width healing
326 (*CWH*) was calculated as shown in Equation 1:

$$CWH = \frac{w_i - w_h}{w_i} \times 100\% \quad (\text{Eq. 1})$$

327

328 where w_i is the initial crack width and w_h is the healed crack width.

329 Visual observations on the specimen surface only provide an indication of the extent of self-healing
330 occurring at the crack mouth and do not provide insight into the healing processes that take place
331 deeper into the crack. Therefore, non-destructive techniques such as the use of ultrasonic wave
332 transmission and air permeability were used to provide information about internal densification and
333 self-healing. An ultrasonic pulse velocity test instrument complying with European standard EN12504-
334 4 and BS1881:Part 203 was used to measure the crack depth at each of the crack observation locations
335 during the monitoring events. The ultrasonic probes were placed on the concrete surface adjacent to
336 the crack and ultrasonic couplant was used between the surfaces to facilitate transmission. Water-
337 saturation of the walls hindered both the ultrasonic and air permeability measurements throughout
338 the monitoring period. Subsequently, only three monitoring events were possible for the former;
339 namely after cracking, at 2 weeks and at 26 weeks (monitoring #1 and #5 respectively) whereas only
340 two for the latter; after cracking and at 26 weeks (monitoring #5). This was due to the consistently
341 high levels of rainfall in the area particularly over the wet winter months.

342 2.3 Microstructural analysis

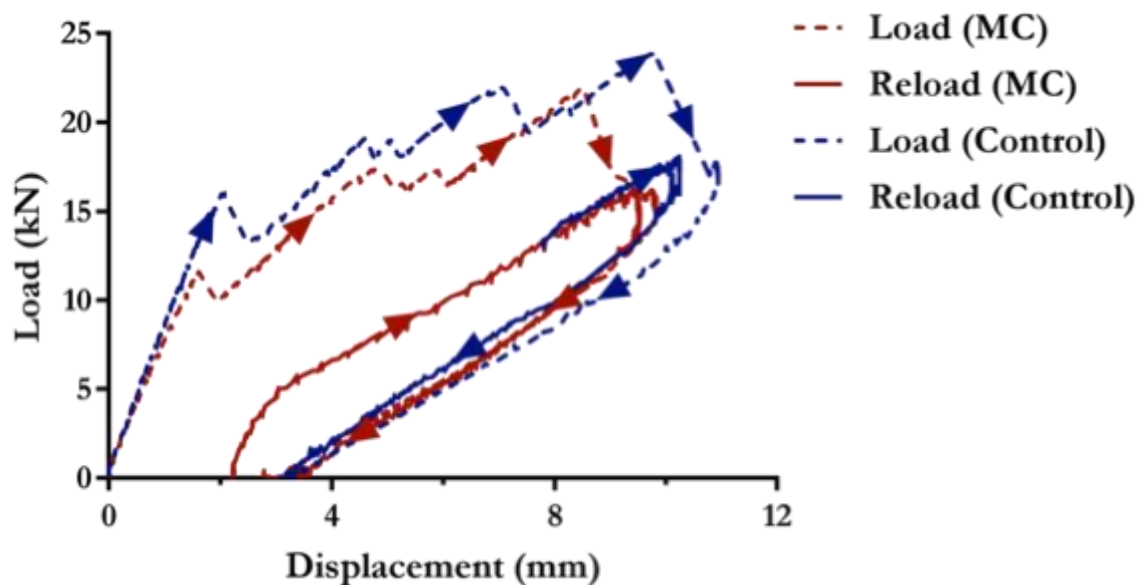
343 Following the re-loading of the wall panels, hence at 6 months, material was extracted from the crack
344 surface after load removal. A multi-tool fitted with a grout removal attachment was used to carve our
345 pieces of materials extract and also powder that was later passed through a 40 μ m sieve for laboratory
346 investigations of the microstructure to quantify the products that formed in the cracks. Tests
347 employed include scanning electron microscopy (SEM), X-ray Diffraction (XRD), thermogravimetric
348 analysis (TGA) and differential thermogravimetric analysis (DTG). In addition, cores 100 mm in
349 diameter and 200 mm high were also cored from the microcapsule wall and tested in a CT scanner to
350 observe the homogeneity of the distribution of the microcapsules within the concrete and how intact
351 they are.

352 3 Results and Discussion

353 3.1 Characteristic strength and mechanical loading

354 The characteristic cube strength obtained of the concrete mixes tested at 28 days without and with
355 microcapsules were 59.3MPa \pm 0.85 and 42.2MPa \pm 3.8 respectively. Although previous lab work [36]
356 had indicated that the addition of microcapsules would have a minimal effect on the strength of the
357 concrete the observed values suggested a strong effect on strength development. It was stipulated
358 that the great variation and discrepancy in results for cube strength for the site mixes is the result of
359 significantly deteriorated workability and honeycombing. The reason for this being the double
360 handling of the concrete to enable the microcapsules to be added to the mix as well as inadequate
361 hand compaction of the cube specimen as a consequence of the casting sequence adopted on site.

362 The load-displacement relationship for both panels for initial loading and reloading seen in Fig. 12
363 confirm that the strength of the panel as not compromised by the addition of the microcapsules. This
364 figure shows that both the initial peak loads obtained, 23.9kN and 21.9kN for the control and
365 microcapsule panels respectively, and the residual loads, 17.4kN and 16.2kN respectively, suggest a
366 smaller decrease (\sim 8%) due to the presence of the microcapsules. Similarly, the concrete stiffness
367 values were also seen to only decrease by \sim 8% from 7.8kN/mm in the control panel to 7.1kN/mm in
368 the microcapsule panel. These results are in better agreement with the cylindrical compressive
369 strength results for microcapsule-loaded concrete samples cast and tested in the laboratory (\sim 9%)
370 [36] as well as previous laboratory observations for mortars [21].

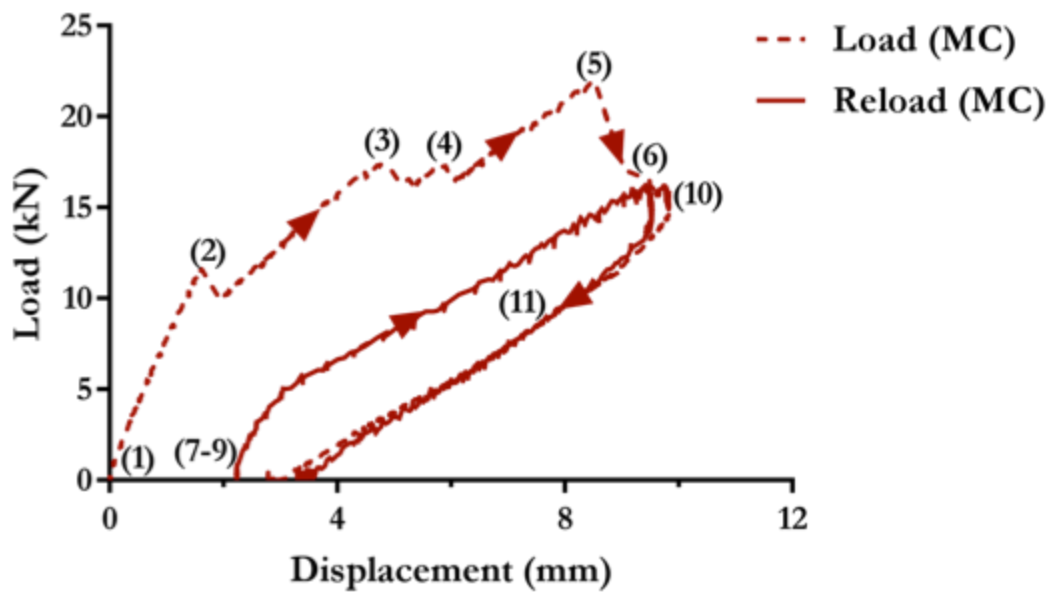


371

372 **Figure 11 Initial and reload load-displacement curves for the microcapsule and Control wall panels.**

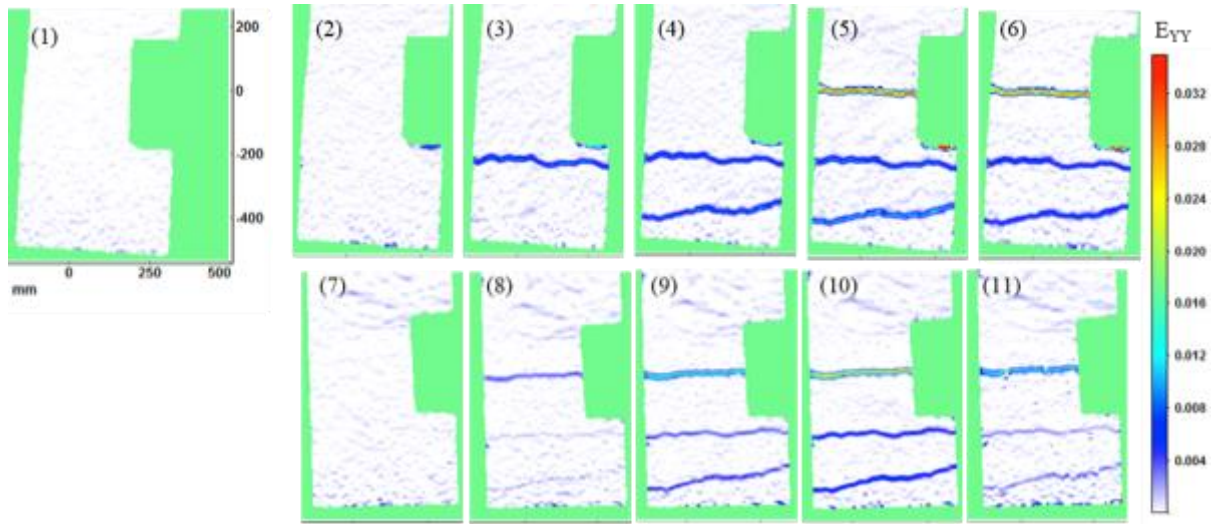
373 Several microcracks were formed during loading, evident from the various drops in the load-
 374 displacement curves (Fig. 12a and 13a). The first crack was noticed at 16.1kN (~72% of maximum load)
 375 and 11.6kN (~55% of maximum load) in the control and microcapsule walls respectively. This
 376 microcracking was also clearly visualised in the DIC images showing vertical strain E_v since loading
 377 induced tensile stresses normal to the plane of the crack (i.e. mode I crack separation). In the
 378 microcapsule panel, a microcrack formed at ~280-300 mm from the base before a second microcrack
 379 formed below this at between 30-100mm (Fig. 12b). In comparison, for the control panel, a microcrack
 380 first formed closer to the base at 50-100mm and then a second between 200-250mm (Fig. 13b).
 381 Despite those differences, two significant microcracks were formed in both walls between the
 382 designed crack location and the wall's joint with the base slab. The third crack was then generated at
 383 the designed location 500mm from the base, resulting in failure of the wall. Due to technical logging
 384 issues, the initial reload curve for the control panel was not obtained.

385 The DIC results show that during reloading it was the main crack that first re-opened before the
 386 opening of the other two microcracks occurred in both the microcapsule (Fig. 12b) and control wall
 387 (Fig. 13b), confirming that low strength regain is possible by autogenic healing or mineral based-
 388 autonomic healing. This is in agreement with previous unconfined compressive strength (UCS) and
 389 flexural laboratory tests on the microcapsule-based concrete system [36] where an addition of 8%
 390 microcapsules achieved 10% more strength than the control and an absolute strength recovery of 25%
 391 over the monitored period.



392
 393
 394

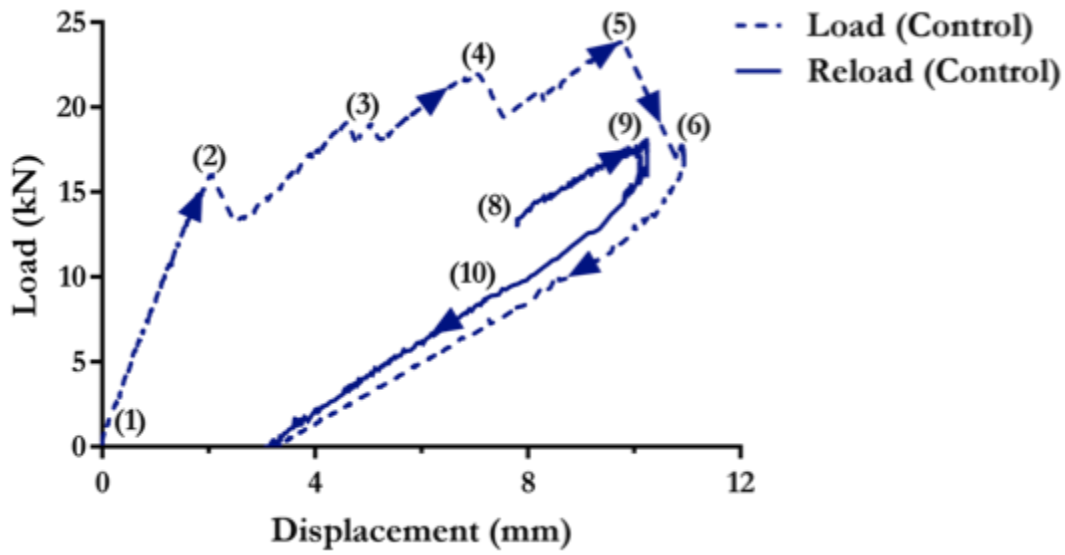
(a)



(b)

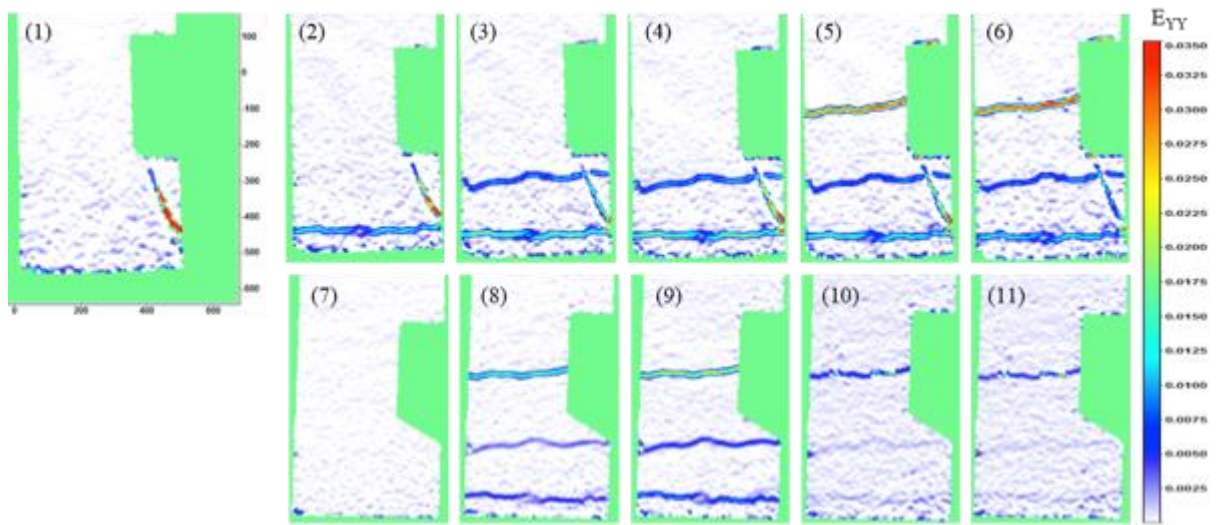
395
396
397
398

Figure 12 (a) Loading and reloading of the microcapsule wall and (b) corresponding DIC images.



(a)

399
400



(b)

401
402

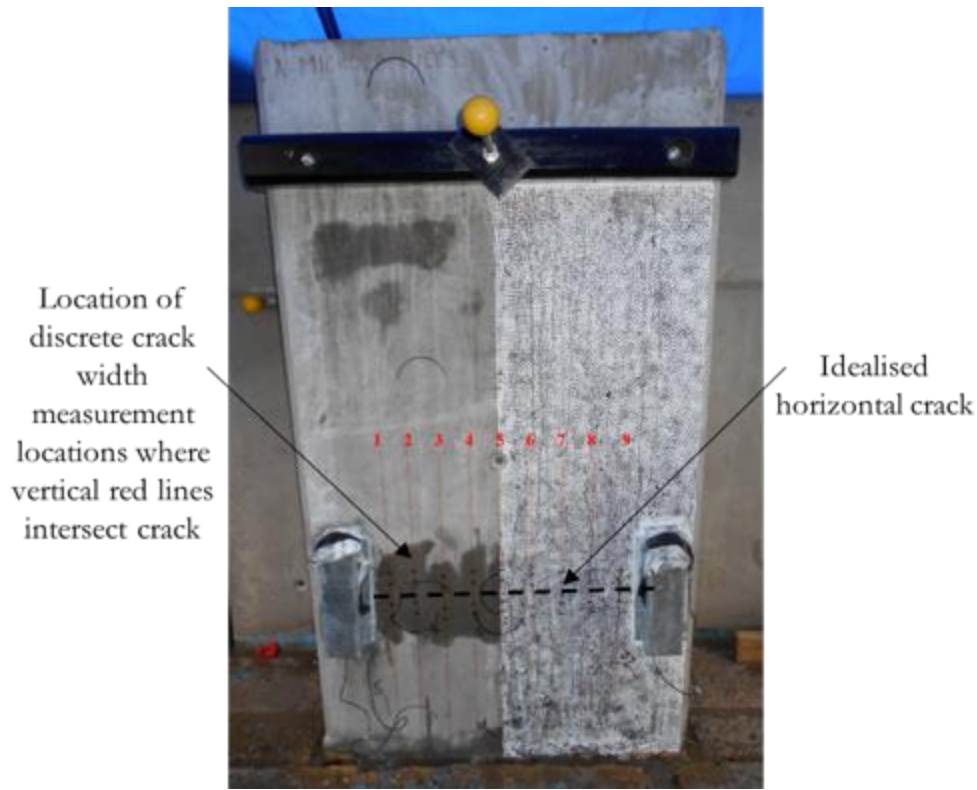
403 **Figure 13 (a) Loading and reloading of control wall and (b) corresponding DIC images.**

404

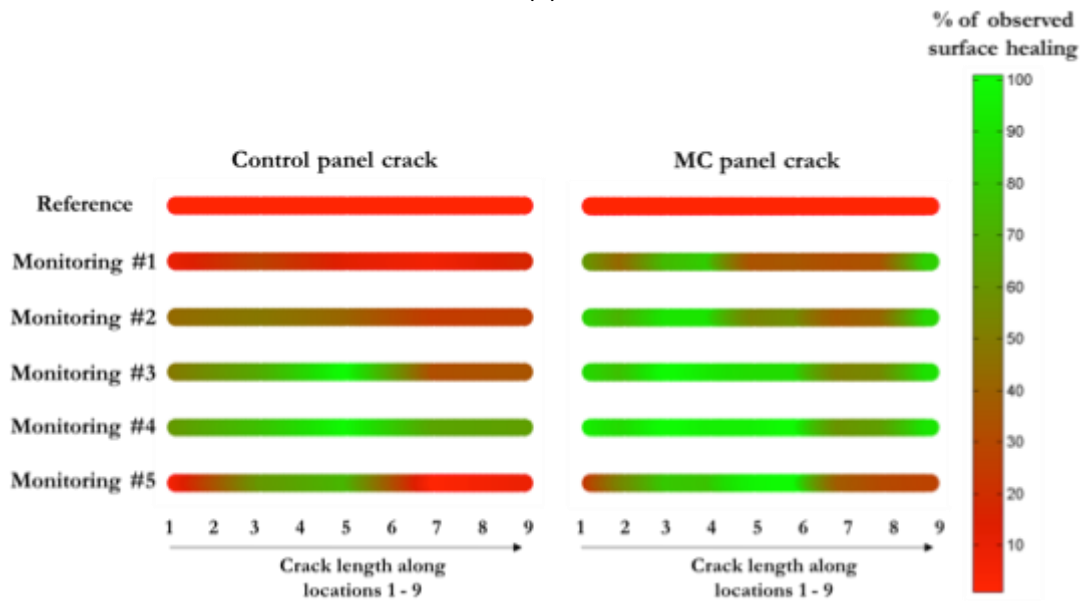
405 3.2 Microscopic crack healing

406 Following initial cracking and subsequent load release, residual crack width measurements were
407 recorded from optical microscope images showing initial average crack widths of 165 μ m and 115 μ m
408 in the control and microcapsule panels respectively, consistent with the lower load reached in the
409 latter. The DEMEC and LVDT crack opening measurements results were comparable with those
410 measured from the microscope images. The progress of healing was monitored throughout the 6-
411 month testing period through microscope imaging of the crack width. During this monitoring period,
412 no reduction in DEMEC and LVDT measurements was observed indicating that any reduction in crack
413 width obtained is not from mechanical re-joining of the crack faces but rather due to the expected
414 healing mechanism of depositions, filling and sealing within the crack.

415 Interpolation of crack width measurements on different locations along the crack length (shown in
416 Fig. 14a) can be seen in Fig. 14b in which the colour-bar indicates the level of crack closure achieved.
417 Similar crack width healing characteristics are seen in both panels with less healing observed on the
418 right-hand side of wall panel due to the paint required for the DIC speckle pattern. The paint has a
419 waterproof characteristic and therefore water runs off the surface rather than permeating into the
420 crack and contributing to clogging of the crack mouth. Accelerated average crack healing along the
421 main crack location, of 49% and 63% was evident as early as monitoring events #1 (14 days) and #2
422 (28 days) for the MC panel compared to 14% and 36% respectively, observed in the Control panel.
423 These results not only confirmed preliminary investigation for mortars specimen [21] but also were in
424 good agreement with microscopic crack width healing reported in laboratory concrete samples
425 prepared with equivalent microcapsule content. The average crack width healing for cube, cylinder
426 and prism concrete specimens after a 28-day water-immersed healing period was established in
427 laboratory conditions prior to the field trials. There, microcapsule-containing samples showed
428 superior crack closure- reaching ~50%, compared to the control samples with an average of less than
429 23% [36]. The large variations in areal healing observed in the control laboratory samples were also
430 consistent with those observed for the Control panel on site.



(a)



(b)

Figure 14 Monitoring crack width healing in panels: (a) microcapsules wall panel showing the locations (numbered 1-9) at which discrete crack width measurements were taken and (b) continuous crack width healing percentage plots for both panels.

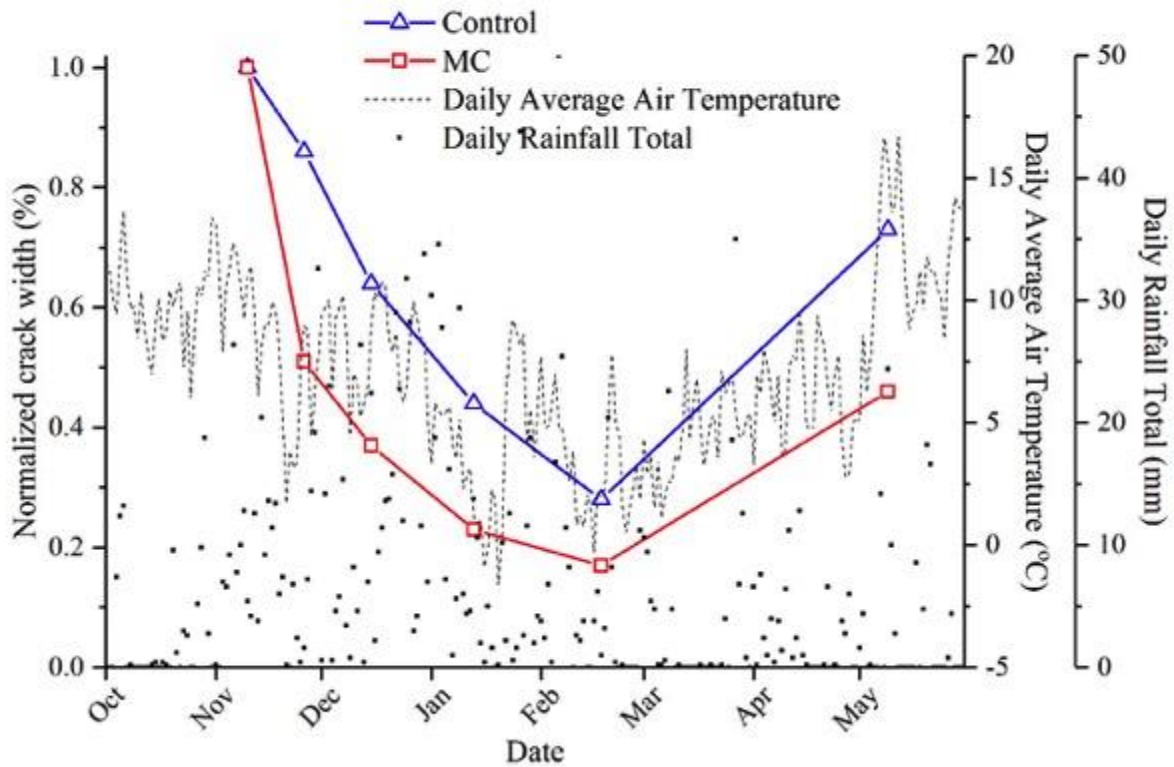
433
434
435
436
437
438

439 Although the observed overall healing was within the expected range with final observed healing of
440 54% and 27% for microcapsule and control wall respectively, a temporal variation of the healing
441 progression between monitoring events was observed in both panels. There is a clear increase in crack
442 opening between monitoring event #4 and #5 for both panels although this is less prominent for the
443 microcapsule wall. Thermal expansion and contraction due to changes in atmospheric temperature

444 contributed to the change in crack width measurements. The mean crack width obtained over the
445 monitoring period can be seen in Fig. 15a along with the daily average air temperature obtained from
446 local weather stations. Crack width measurements are normalised with respect to the width obtained
447 following load removal (i.e. residual crack widths). A trend is clearly observed between the daily
448 average air temperature and the normalised crack width in both the microcapsule and control panels.
449 Crack width measurements constantly reduced during the first four monitoring events (between
450 November 2015 and February 2016). However, the normalised crack width increased for the final
451 monitoring event before reloading of the panels in May 2016 although the measured width is still less
452 than the residual crack width measured upon initial loading of both panels. This indicates that
453 variations in measured crack width cannot be solely due to thermal expansion and contraction but
454 also due to self-healing contributions.

455 The crack in the microcapsule wall shows consistently greater closure than in the control wall
456 throughout the monitoring period. In particular, the initial crack closure (indicated by the negative
457 slope between the first and second measurements) is higher for the microcapsule panel. This indicates
458 that the autonomic self-healing reactions have begun within the first two weeks after cracking. Studies
459 that have explored the efficacy of sodium silicate as a healing agent have observed mechanical binding
460 of sodium silicate with hardened cement paste [16,38] even within 48 hours [39]. It is no surprise
461 therefore, that the autonomic self-healing benefit is realised within the first two weeks of cracking.
462 Since temperatures did fall below 0°C in January and February, freeze-thaw damage may also have
463 contributed to the observed behaviour. Free water that freezes within the concrete pores expands
464 and exerts internal stresses to the material. These stresses may drive open pre-existing microcracks
465 (thereby increasing the observed crack width) or may create new cracks in the material. Cycles of
466 freeze-thaw can cause progressive and cumulative damage.

467 Observations of daily rainfall totals also suggest the contribution of rainwater to the healing process.
468 Fig 15b shows the average normalised crack width along with daily rainfall totals. The greatest amount
469 of rainfall is observed during the first three months after initial cracking; namely in December, January
470 and February. Water is necessary for the reaction of the released sodium silicate with the hardened
471 cement matrix. Furthermore, the presence of water is one of the most important criteria for successful
472 autogenic self-healing [40,41]. The temporary addition of insulation to the microcapsule panel in the
473 first two weeks of monitoring did not appear to have affected the obtained results. Theoretically, less
474 self-healing is expected in the locations that were covered due to water deprivation in the cracks
475 limiting both autogenic and autonomic self-healing processes. However, in this wet environment, the
476 insulation tape was inadequate to provide protection from rainwater and the concrete quickly
477 saturated under rainy conditions.



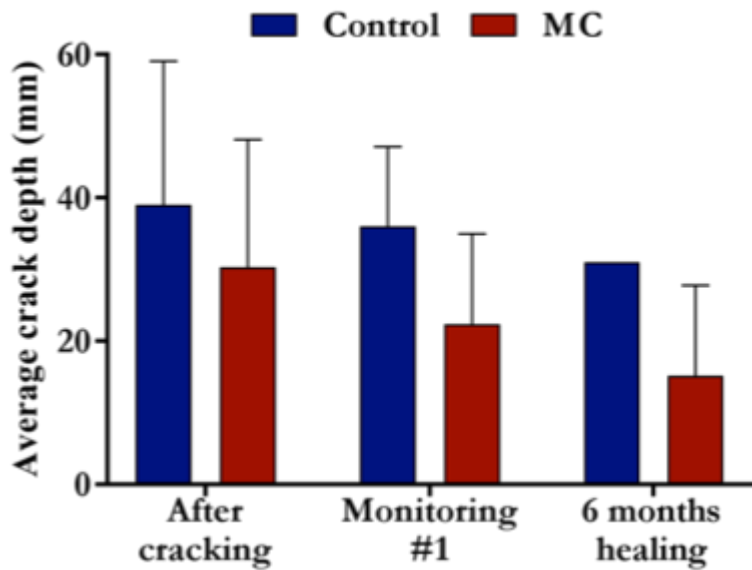
478

479 **Figure 15 Monitoring crack width healing in panels: (a) microcapsules wall panel showing the**
 480 **locations (numbered 1-9) at which discrete crack width measurements were taken and (b)**
 481 **continuous crack width healing percentage plots for both panels.**

482

483 3.3 Crack depth and permeability

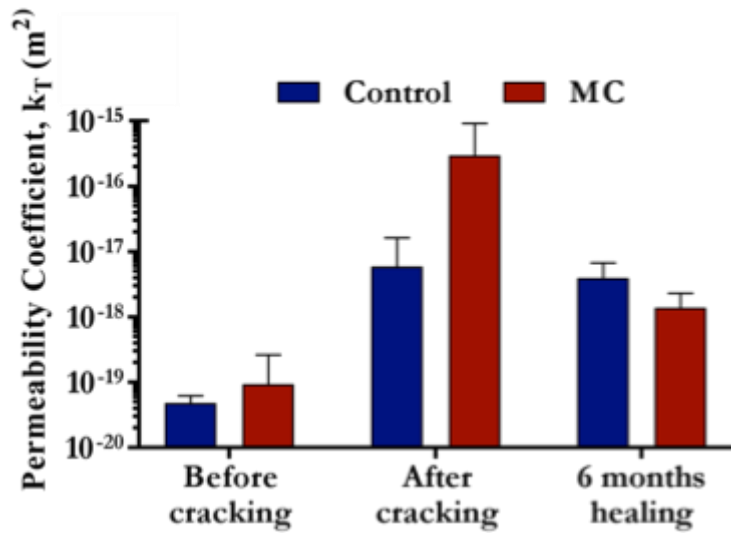
484 The crack depth measurements taken with the ultrasonic device on site are presented in Fig. 16. Only
 485 three monitoring events were possible; after cracking, after 2 weeks and after 26 weeks (monitoring
 486 #1 and #5 respectively) due to a number of challenges faced with the testing on site, since
 487 measurements were unreliable when the surface of the concrete was wet. In addition, the uneven
 488 wall surface made the use of probes quite problematic. The average crack depth reduced by ~8% and
 489 ~39% after 2 weeks (#1) and ~20% and ~58% after 26 weeks of healing (#5), in the control and
 490 microcapsule walls respectively. Interestingly, the observed relative improvement by the addition of
 491 microcapsules is higher compared to laboratory measurements (~28%) on concrete samples produced
 492 with the same dosage of microcapsules.



493

494 **Figure 16 Average ultrasonic crack depth measurements after cracking, after 2 weeks and after a**
 495 **6-month healing period.**

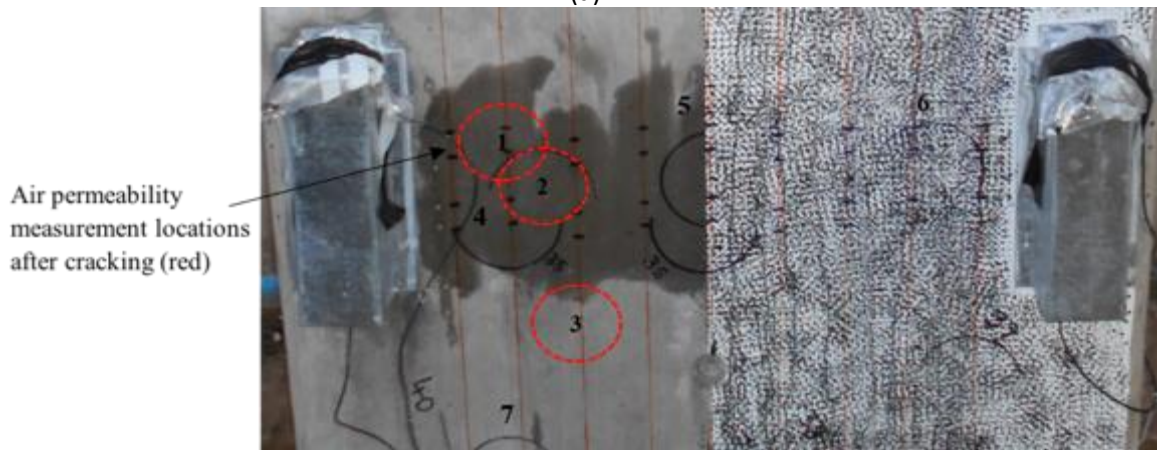
496 The coefficient of air permeability values measured at three periods are shown in Fig. 17a, showing
 497 very similar values of $\sim 10^{-19}$ kT for both walls before cracking suggesting that the microcapsules did not
 498 significantly alter the initial porosity of the concrete. This value is typical for concrete of very low
 499 permeability [42]. After cracking, the air permeability of the microcapsule wall was noticeably greater
 500 than the control wall by ~ 2 orders of magnitude. Since the microcapsule wall failed at $\sim 8\%$ lower load
 501 than the control panel and hence slightly weaker, it is possible that this had induced a greater content
 502 of internal microscale damage and cracking. It should be noted here, that it was not possible to obtain
 503 air permeability measurements after cracking from all of the same locations prior to cracking. When
 504 placing the device in locations directly over the induced crack, the device was unable to create a
 505 vacuum and therefore obtain a reasonable measurement. Since the crack passed through the initial
 506 measurement locations, new locations adjacent to previous measurement locations were chosen (Fig.
 507 17b). At monitoring stage #5 (6 months of healing), the permeability of the control panel reduced only
 508 slightly, while that for the microcapsule wall recovered significantly, by >2.5 orders of magnitude, to
 509 $\sim 10^{-18}$ kT. The permeability of the microcapsule wall was half an order of magnitude less than the
 510 control wall and was consistent with trends observed in the laboratory using sorptivity tests. The
 511 average sorptivity coefficients calculated across control and microcapsule-containing concrete
 512 samples after a 28-day healing period show that the rate of water absorption by microcapsule loaded
 513 samples is generally lower than that of the control [36]. Nonetheless the permeability of both walls
 514 remained greater than the permeability prior to cracking indicating only partial self-healing at that
 515 stage.



516

517

(a)



518

519

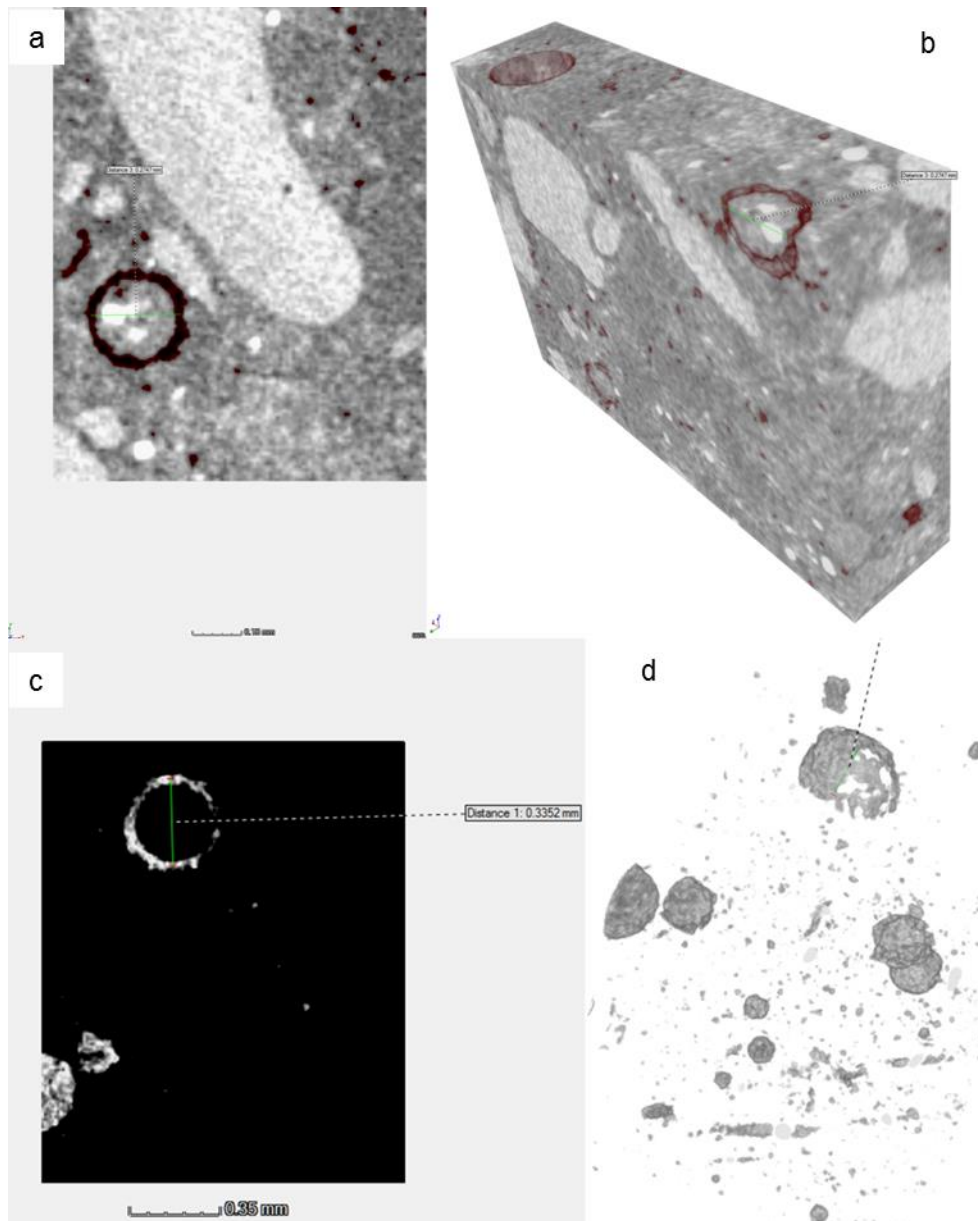
(b)

Figure 17 (a) Permeability of wall panels before cracking, after cracking and after a 6-month healing period and (b) Air permeability measurement locations after loading and subsequent cracking of concrete wall panel.

523

524 3.4 Microstructural analysis

525 Extracted cores were placed in a CT scanner and a typical image is shown in Figure 18. The figure and
 526 a detailed assessment of the CT scan images throughout the sample, confirmed uniform distribution
 527 of the microcapsules and their intact nature. The shell material was associated with a circular shaped
 528 low density material filled with a solid material, as shown in Fig. 18. The circular shape was typically
 529 ~250-350 μm , similar size to the microcapsules. As the material is filled with a solid, and not air, we
 530 believe that the microcapsules have maintained their functionality yet the core material initially liquid,
 531 may have solidified in the time of investigation. Namely the osmotic difference has attracted gradually
 532 the water molecules outside of the shell wall to the surrounding matrix. Hence the solid/crystalline
 533 sodium silicate (the healing agent) is still within the microcapsules but not in its original liquid state.



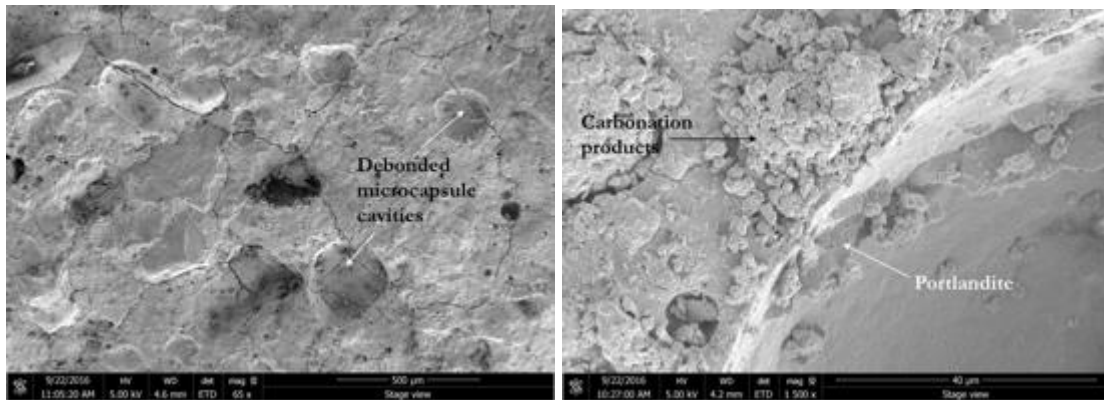
534

535 **Figure 18** μ CT scan image of a core from the microcapsule wall.

536 Extracted materials of the crack surface from both panels were observed using an SEM to characterise
 537 the healing products and typical images are presented in Fig. 19a-e. Fig. 19a shows multiple smooth
 538 cavities left by either debonded or ruptured microcapsules together with microcracks throughout the
 539 image attracted to, and passing through, the microcapsule locations. This is in agreement with
 540 previous observations whereby the presence of microcapsules were seen to provide a preferential
 541 path for cracks in mortar [21]. This phenomenon is considered beneficial for this self-healing system
 542 as it ensured microcapsules can be ruptured during crack propagation. Fig. 19b shows hexagonal
 543 calcium hydroxide crystals indicating their formation in the periphery of the microcapsules although
 544 on the crack surface, little, if any, can be seen. Instead, calcium carbonate and copious C-S-H flakes
 545 were observed. The former of these observations agree with previous findings that microcapsules act
 546 as nucleation sites for portlandite formation [43] whilst the latter of these products may be attributed
 547 to the reaction of the encapsulated sodium silicate with portlandite [39].

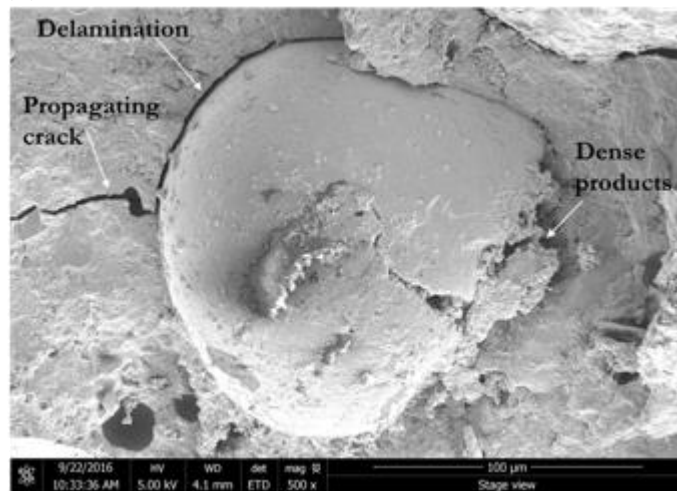
548 As the pieces of concrete material were extracted from near the crack mouth, the increased quantity
 549 of observed carbonation products is not surprising due to direct exposure to the external environment
 550 and CO_2 . SEM images also show products that have precipitated within small spherical voids of

551 entrained air (Fig. 19b) suggesting that the products were generated following hardening of the
 552 concrete and most likely not produced during the initial cement hydration process. Ruptured
 553 microcapsules embedded on the crack surface could also be seen. In Fig. 19c, a crack approaching
 554 from the left-hand side is seen to pass through, or potentially debond, the microcapsule at this
 555 location. The stress concentration generated by the crack at this point was clearly not sufficient to
 556 rupture the microcapsule shell. However, on the right-hand side, the microcapsule shell is certainly
 557 ruptured and copious dense amorphous calcium silicate hydrate (C-S-H) phases are observed in the
 558 vicinity as suggested by the image brightness. In contrast, SEM images of samples extracted from the
 559 control panel (e.g. Fig. 19d and 19e) are consistently darker than those obtained from the
 560 microcapsule panel; indicating higher porosity in the matrix. The SEM images also show a variety of
 561 cement hydration products. Large calcium hydroxide crystals can be seen with other carbonation and
 562 C-S-H products on top. All of these SEM observations agree well with the expected autonomic self-
 563 healing mechanism whereby sodium silicate reacts with portlandite to produce C-S-H.



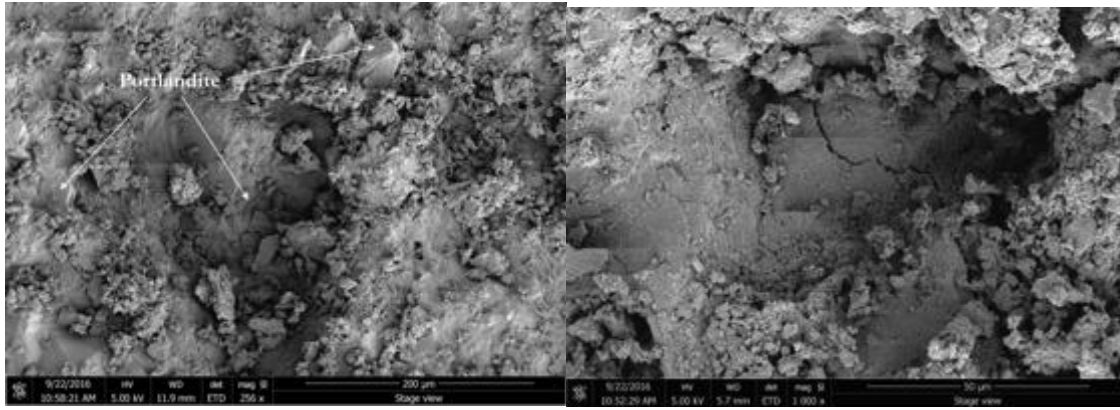
564
 565

(a) (b)



566
 567

(c)



(d)

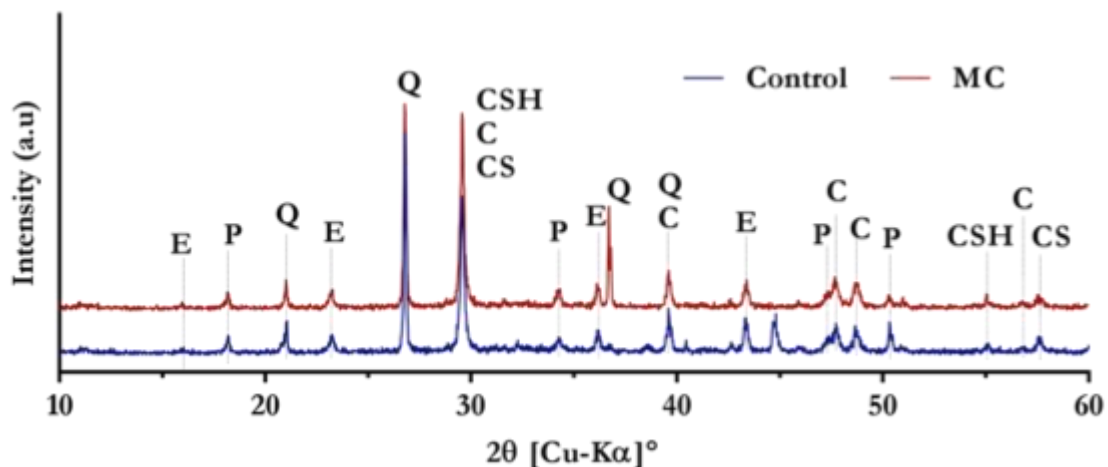
(e)

568

569

570 **Figure 19 Scanning electronic microscope (SEM) images from the MC and Control wall crack**
 571 **surfaces: (a) the attraction of microcracks towards microcapsule cavity locations; (b) crack surface**
 572 **adjacent to microcapsule cavity showing the deposition of carbonation and hydration products; (c)**
 573 **a ruptured microcapsule with dense hydration products at the outlet and (d, e) crack surface of the**
 574 **control wall showing high porosity and copious carbonation products.**

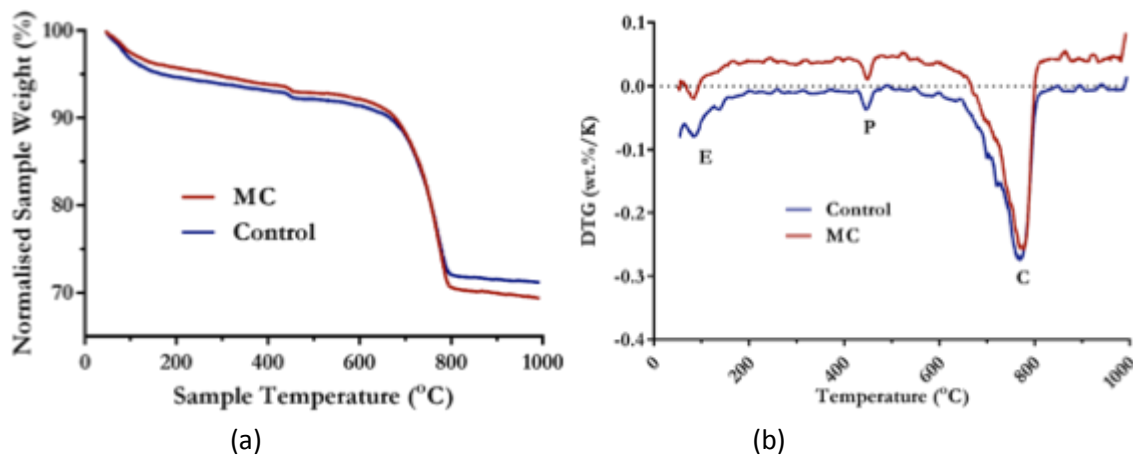
575 XRD spectra for material extracted from both the microcapsule and control wall cracks after reloading
 576 revealed the same crystalline materials within the powdered samples, e.g. portlandite C-H, calcite and
 577 broad C-S-H peaks, with marginal differences observed (Fig. 20). This confirms that similar products
 578 have formed in the cracks. TGA/DTG tests (Fig. 21) showed similar quantities of portlandite and calcite
 579 with the portlandite content being quite very small. This is consistent with the SEM observations and
 580 is expected as portlandite close to the wall surface will carbonate to produce calcite. As mentioned
 581 previously, it has been observed that the portlandite content in cementitious samples increases when
 582 microcapsules are added into the mixture. Therefore, before damage occurs, an increased quantity of
 583 portlandite in expected to exist within the MC wall compared with the Control wall. However, when
 584 damage occurs and microcapsules are ruptured, sodium silicate is released and reacts with portlandite
 585 to produce C-S-H. Therefore, the portlandite content within a crack, and particularly in the vicinity of
 586 microcapsules, should reduce. As a result, the similar quantities of portlandite measured could
 587 actually indirectly suggest that the autonomic self-healing reactions did take place. The larger
 588 quantities of calcite measured in samples extracted from the microcapsule wall also support these
 589 observations. The larger quantities suggest that a greater proportion of portlandite existed previously
 590 in this region and ultimately in the microcapsule wall.



591

592 **Figure 18 X-ray power diffraction (XRD) of powder extracted from MC and Control wall crack, where**
 593 **C: CaCO₃, CS: 2CaO·SiO₂, 3CaO·SiO₂, CSH: 3CaO·2SiO₂·4H₂O, P: Ca(OH)₂ and Q: SiO₂.**

594



595

596

597 **Figure 19 Representative TGA/DTG graphs of powder extracted from crack faces of MC and control**
598 **walls (a) TGA weight loss, (b) DTG curves where E: ettringite, P: portlandite and C: calcite**

599 It is worth noting that it is difficult to distinguish between a reduction in portlandite due to reaction
600 with the sodium silicate or carbonation to form calcite. However, these cumulative measurements
601 support the hypothesis that a greater portlandite content existed in the microcapsule wall prior to
602 cracking and has either been converted to calcite or reacted with the healing agent to form C-S-H.
603 Furthermore, the increased quantity of calcite measured in the microcapsule wall sample is consistent
604 with the increased visual healing that was observed at the crack mouth.

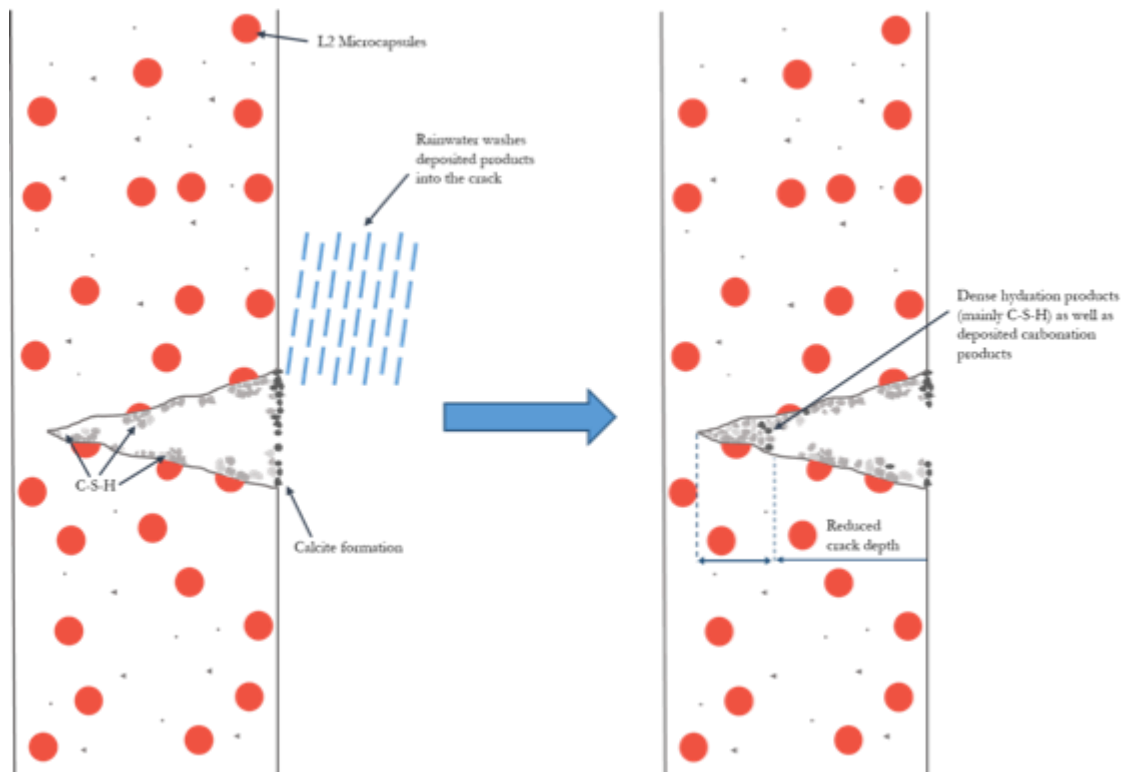
605

606 3.5 Healing mechanism

607 Coupling non-destructive testing results with macroscopic and microscopic observations it is possible
608 to theorise the self-healing mechanism that had taken place in both walls. In both walls, the observed
609 width at the crack mouth consistently reduced between monitoring events #1 and #4, mainly due to
610 the precipitation of calcite. These monitoring events took place between November and February
611 whereby air temperatures gradually decreased and daily rainfall increased. However, between
612 monitoring events #4 and #5, less carbonates filled the crack mouth and the measured crack width
613 increased. It is believed that the increased rainfall washed products that had precipitated at the crack
614 mouth deeper into the crack and towards the crack tip (shown schematically in Fig. 22). The crack
615 depth measurements taken at monitoring event #5 (Fig. 16) support this. However, the reduction in
616 crack depth was also caused by autogenic healing at the crack tip. At this location, healing was most
617 likely to occur due to the close proximity of fracture surfaces. TGA of healing products on the crack
618 surface and at the crack mouth revealed the large quantity of calcite present. In particular, a greater
619 quantity of calcite was observed in the microcapsule wall crack. This is in agreement with the crack
620 width observations in which the microcapsule wall saw greater areal healing. Since greater quantities
621 of calcite precipitated at the crack mouth, a greater amount was washed into the crack. Therefore,
622 greater healing at the crack mouth resulted in greater healing at the crack tip. However, these results
623 also showed that healing at the crack mouth did not necessarily correspond to healing inside the crack.

624 The significant reduction in crack depth in the microcapsule wall hence cannot be due to the
625 deposition of calcite alone. As well as the contribution from autogenic healing, autogenic healing due
626 to the release of microencapsulated sodium silicate occurred. Microcapsules on the crack surface that
627 were embedded within the cementitious matrix showed rupture and formed dense hydration
628 products at the outlet. TGA results also showed a greater degree of hydration for the microcapsule
629 wall; suggesting more hydration processes had occurred in comparison with the Control panel. Finally,
630 air permeability measurements taken around the crack location also showed significant healing for
631 the microcapsule wall in comparison to almost no healing in the Control wall (Fig. 17). These results

632 are particularly useful as they provide insight into the densification of the bulk material due to self-
633 healing processes taking place internally at other microcrack locations.



634
635 **Figure 22 Healing mechanism of concrete wall panels: Carbonation products at the crack mouth are**
636 **washed into the crack. This, along with autogenic and autonomic healing along the crack length and**
637 **tip lead to a reduction in crack depth measurements.**

638 4 Conclusions

639 The work presented here is part of the first major self-healing concrete site trial in the UK. It is the first
640 successful attempt to scale up and implement self-healing concrete incorporating microcapsules on
641 site. Self-healing concrete using microencapsulated sodium silicate was cast on-site in a retaining wall
642 panel together with a control panel for comparison purposes. The walls were mechanically cracked
643 after 35 days of curing and then reloaded and monitored for self-healing over a 6-month period using
644 air permeability, crack depth and microscopic crack width measurements. Although the addition of
645 8% microcapsules, by volume of the cement, was found to slightly reduce the mechanical strength,
646 the microcapsule wall showed improved crack-width reduction, crack-depth reduction and recovery
647 in permeability, confirming the real-time feasibility of microcapsule-based healing. In particular:

- 648 • Accelerated crack healing along the main crack of 49% and 63% was evident as early as 14
649 days and 28 days for the microcapsule wall compared to 14% and 36% respectively for the
650 control.
- 651 • The average crack depth was also seen to reduce by ~8% and ~39% after 14 days in the control
652 and microcapsule walls respectively reaching a final ~20% and ~58% at the end of the
653 monitoring period.
- 654 • These results were further confirmed by significant permeability recovery (almost greater
655 than 2.5 orders of magnitude) for the microcapsule wall.
- 656 • A strength recovery of 25% was achieved in the microcapsule wall, achieving a 10%
657 improvement over the control panel.
- 658 • A temporal variation of the healing progression was identified in both panels influencing final
659 observations. Macroscopic observations showed some crack opening for both walls following

660 the initial reduction in crack width. Yet healing at the end of the monitoring period for the
661 microcapsule panel remained significantly higher compared to the control panel.
662 • Microscopic imaging and microstructural investigations of extracted samples from the crack
663 planes suggested a self-healing mechanism similar to what was observed in laboratory
664 investigations.
665 • μ CT confirmed the survivability and good distribution of microcapsules on site. SEM images
666 revealed dense products formed around embedded ruptured microcapsules confirming the
667 hypothesised release mechanism.
668 • TGA and XRD results of extracted material from the crack surfaces showed copious
669 carbonation products in both cases and increased quantities of calcium silicate hydrate (C-S-
670 H) in the microcapsule wall further supporting previous findings on the beneficial contribution
671 of the microencapsulated sodium silicate to the autonomic self-healing progress.

672 Although the cast panels were not used in a structural application, this is a valuable step in gaining the
673 confidence of civil engineering contractors, designers and consultants to adopt disruptive
674 technologies working towards reducing and removing the requirement for inspection, maintenance
675 and repair of concrete structures.

676 Conflict of Interest

677 None.

678 Acknowledgements

679 The authors would like to thank all of those involved with the EPSRC Materials for Life (M4L) project;
680 in particular, Dr Robert Davies, Dr Martins Pilegis and Dr Oliver Teal for their contribution to the field
681 trials. The financial support from the EPSRC for the Materials for Life (M4L) project (EP/K026631/1)
682 and Resilient Materials for Life (RM4L) Programme Grant (EP/P02081X/1) is gratefully acknowledged.
683 The financial support from the EPSRC in the form of PhD studentships to Petros Giannaros and
684 Chrysoula Litina is also gratefully acknowledged.

685 References

- 686 [1] UK Treasury, National Infrastructure Delivery Plan 2016–2021, HM Treasury, London,
687 2016. www.gov.uk/government/publications.
- 688 [2] ONS, Construction output in Great Britain: May 2016, (2016).
689 <https://www.ons.gov.uk/>.
- 690 [3] G. Tilly, J. Jacobs, Concrete repairs: Performance in service and current practice, BRE
691 Press, UK., 2007.
- 692 [4] World Economic Forum, The Boston Consulting Group, A Breakthrough in Mindset
693 and Technology - Shaping the Future of Construction, 2016.
- 694 [5] European Commission, Business Innovation Observatory - Smart Living: Advanced
695 Building Materials, 2014.
- 696 [6] Government Office For Science, Technology and Innovation Futures, 2017.
- 697 [7] i3P, Technology Roadmap for UK Construction & National Infrastructure, 2017.
698 [https://www.i3p.org.uk/wp-content/uploads/2017/07/i3P-CI-Technology-Roadmap-Booklet-](https://www.i3p.org.uk/wp-content/uploads/2017/07/i3P-CI-Technology-Roadmap-Booklet-FINAL.pdf)
699 [FINAL.pdf](https://www.i3p.org.uk/wp-content/uploads/2017/07/i3P-CI-Technology-Roadmap-Booklet-FINAL.pdf).
- 700 [8] M. de Rooij, K. Van Tittelboom, N. De Belie, E. Schlangen, Self-Healing Phenomena in
701 Cement-Based Materials State-of-the-Art Report of RILEM Technical Committee 221-SHC: Self-
702 Healing Phenomena in Cement-Based Materials, RILEM 2013, 2013.
- 703 [9] N. De Belie, E. Gruyaert, A. Al-Tabbaa, P. Antonaci, C. Baera, D. Bajare, A. Darquennes,
704 R. Davies, L. Ferrara, T. Jefferson, C. Litina, B. Miljevic, A. Otlewska, J. Ranogajec, M. Roig-Flores,
705 K. Paine, P. Lukowski, P. Serna, J.-M. Tulliani, S. Vucetic, J. Wang, H.M. Jonkers, A Review of
706 Self-Healing Concrete for Damage Management of Structures, *Adv. Mater. Interfaces*. (2018)

707 1800074. doi:10.1002/admi.201800074.

708 [10] L.L. Souza, A. Al-Tabbaa, Microfluidic fabrication of microcapsules tailored for self-
709 healing in cementitious materials, *Constr. Build. Mater.* 184 (2018) 713–722.
710 doi:10.1016/J.CONBUILDMAT.2018.07.005.

711 [11] B. Boh, Boštjan Šumiga, B. Šumiga, Microencapsulation technology and its
712 applications in building construction materials, *RMZ - Mater. Geoenvironment.* 55 (2008) 329–
713 344.

714 [12] S.R. White, N.R. Sottos, P.H. Geubelle, J.S. Moore, M.R. Kessler, S.R. Sriram, E.N.
715 Brown, S. Viswanathan, Autonomic healing of polymer composites., *Nature.* 409 (2001) 794–
716 7. doi:10.1038/35057232.

717 [13] M. Pelletier, R. Brown, A. Shukla, A. Bose, Self-healing concrete with a
718 microencapsulated healing agent, Kingston, USA, 2011.
719 http://energetics.chm.uri.edu/system/files/Self_healing_concrete_-7-11.pdf.%0A[9].

720 [14] Z. Yang, J. Hollar, X. He, X. Shi, A self-healing cementitious composite using oil
721 core/silica gel shell microcapsules, *Cem. Concr. Compos.* 33 (2011) 506–512.
722 doi:10.1016/j.cemconcomp.2011.01.010.

723 [15] L. Ferrara, T. Van Mullem, M.C. Alonso, P. Antonaci, R.P. Borg, E. Cuenca, A. Jefferson,
724 P.-L. Ng, A. Peled, M. Roig-Flores, M. Sanchez, C. Schroefl, P. Serna, D. Snoeck, J.M. Tulliani, N.
725 De Belie, Experimental characterization of the self-healing capacity of cement based materials
726 and its effects on the material performance: A state of the art report by COST Action SARCOS
727 WG2, *Constr. Build. Mater.* 167 (2018) 115–142. doi:10.1016/j.conbuildmat.2018.01.143.

728 [16] A. Kanellopoulos, T.S. Qureshi, A. Al-Tabbaa, Glass encapsulated minerals for self-
729 healing in cement based composites, *Constr. Build. Mater.* 98 (2015) 780–791.
730 doi:10.1016/j.conbuildmat.2015.08.127.

731 [17] T.S. Qureshi, A. Kanellopoulos, A. Al-Tabbaa, Encapsulation of expansive powder
732 minerals within a concentric glass capsule system for self-healing concrete, *Constr. Build.*
733 *Mater.* 121 (2016) 629–643. doi:10.1016/J.CONBUILDMAT.2016.06.030.

734 [18] C. Litina, A. Kanellopoulos, A. Al-Tabbaa, Alternative repair system for concrete using
735 microencapsulated healing agents, in: M. Grantham, M. Basheer, B. Magee, M. Soutsos (Eds.),
736 *Proc. Concr. Solut. 5th Int. Conf. Concr. Repair*, Taylor & Francis Group, Belfast, 2014: pp. 97–
737 103.

738 [19] A. Kanellopoulos, P. Giannaros, D. Palmer, A. Kerr, A. Al-Tabbaa, Polymeric
739 microcapsules with switchable mechanical properties for self-healing concrete: synthesis,
740 characterisation and proof of concept, *Smart Mater. Struct.* 26 (2017) 045025.
741 doi:10.1088/1361-665X/aa516c.

742 [20] P. Giannaros, A. Kanellopoulos, A. Al-Tabbaa, Sealing of cracks in cement using
743 microencapsulated sodium silicate, *Smart Mater. Struct.* 25 (2016) 084005. doi:10.1088/0964-
744 1726/25/8/084005.

745 [21] A. Kanellopoulos, P. Giannaros, A. Al-Tabbaa, The effect of varying volume fraction of
746 microcapsules on fresh, mechanical and self-healing properties of mortars, *Constr. Build.*
747 *Mater.* 122 (2016) 577–593. doi:10.1016/j.conbuildmat.2016.06.119.

748 [22] C.M. Dry, Repair and prevention of damage due to transverse shrinkage cracks in
749 bridge decks, 1999 Symp. *Smart Struct. Mater.* 3671 (1999) 253–256.

750 [23] T.D.P. Thao, Quasi-brittle self-healing materials: numerical modelling and applications
751 in civil engineering, PhD Thesis National University of Singapore, 2011.

752 [24] G. Karaiskos, E. Tsangouri, D.G. Aggelis, K. Van Tittelboom, N. De Belie, D. Van
753 Hemelrijck, Performance monitoring of large-scale autonomously healed concrete beams
754 under four-point bending through multiple non-destructive testing methods, *Smart Mater.*
755 *Struct.* 25 (2016). doi:10.1088/0964-1726/25/5/055003.

756 [25] C. Dry, IN-SERVICE REPAIR OF HIGHWAY BRIDGES AND PAVEMENTS BY INTERNAL
757 TIME-RELEASE REPAIR CHEMICALS, NCHRP-IDEA Progr. Proj. Final Rep. (2001).

758 <https://trid.trb.org/view.aspx?id=692570> (accessed October 24, 2017).

759 [26] C.M. Dry, Self-repair of cracks in brittle material systems, in: SPIE 9800, Behav. Mech.
760 Multifunct. Mater. Compos. 2016, Las Vegas, 2016. doi:10.1117/12.2218564.

761 [27] H.M. Jonkers, E. Schlangen, Self-healing of cracked concrete: A bacterial approach,
762 6th Int. Conf. Fract. Mech. Concr. Concr. Struct. 3 (2007) 1821–1826.

763 [28] E. Tziviloglou, V. Wiktor, H.M. Jonkers, E. Schlangen, Bacteria-based self-healing
764 concrete to increase liquid tightness of cracks, Constr. Build. Mater. 122 (2016) 118–125.
765 doi:10.1016/j.conbuildmat.2016.06.080.

766 [29] M.G. Sierra-Beltran, H.M. Jonkers, M. Ortiz, Field application of self--healing concrete
767 with natural fibres as linings for irrigation canals in Ecuador, Fifth Int. Conf. Self-Healing Mater.
768 (2015) 32.

769 [30] A. Stewart, The ‘living concrete’ that can heal itself, CNN. (2016).
770 <https://edition.cnn.com/2015/05/14/tech/bioconcrete-delft-jonkers/index.html>.

771 [31] K. Paine, R. Lark, A. Al-Tabbaa, Biomimetic multi-scale damage immunity for concrete,
772 in: UKIERI Concr. Congr. Concr. Res. Driv. Profit Sustain., Jalandhar (Punjab), India, 2015.
773 <http://opus.bath.ac.uk/48322/>.

774 [32] R.J. Lark, A. Al-Tabbaa, K. Paine, Biomimetic multi-scale damage immunity for
775 construction materials : M4L Project overview, in: 4th Int. Conf. Self-Healing Mater., Ghent,
776 2013: pp. 2–5.

777 [33] A. Al-Tabbaa, B. Lark, K. Paine, T. Jefferson, C. Litina, D. Gardner, T. Embley,
778 Biomimetic Cementitious Construction Materials for Next Generation Infrastructure, Proc. Inst.
779 Civ. Eng. - Smart Infrastruct. Constr. (2018) 1–35. doi:10.1680/jsmic.18.00005.

780 [34] O. Teall, R. Davies, M. Pilegis, A. Kanellopoulos, T. Sharma, K. Paine, A. Jefferson, R.
781 Lark, D. Gardner, A. Al-Tabbaa, Self-healing concrete full-scale site trials, in: K. Maekawa, A.
782 Kasuga, J. Yamazaki (Eds.), Proc. 11th Fib Int. PhD Symp. Civ. Eng., Tokyo, Japan, 2016: pp. 639–
783 646.

784 [35] R. Davies, O. Teall, M. Pilegis, A. Kanellopoulos, T. Sharma, A. Jefferson, D. Gardner,
785 A. Al-Tabbaa, K. Paine, R.J. Lark, Large Scale Application of Self-Healing Concrete: Design,
786 Construction and Testing, Front. Mater. 5 (2018) 51. doi:10.3389/FMATS.2018.00051.

787 [36] P. Giannaros, A. Kanellopoulos, A. Al-Tabbaa, Damage recovery in self-healing
788 concrete, in: Heal. Conf., Delft, The Netherlands, 2016.

789 [37] R.J. Torrent, A two-chamber vacuum cell for measuring the coefficient of permeability
790 to air of the concrete cover on site, Mater. Struct. 25 (1992) 358–365.
791 doi:10.1007/BF02472595.

792 [38] R. Alghamri, A. Kanellopoulos, A. Al-Tabbaa, Impregnation and encapsulation of
793 lightweight aggregates for self-healing concrete, Constr. Build. Mater. 124 (2016) 910–921.
794 doi:10.1016/j.conbuildmat.2016.07.143.

795 [39] S. Irico, A. Bovio, G. Paul, E. Boccaleri, D. Gastaldi, L. Marchese, L. Buzzi, F. Canonico,
796 A solid-state NMR and X-ray powder diffraction investigation of the binding mechanism for
797 self-healing cementitious materials design: The assessment of the reactivity of sodium silicate
798 based systems, Cem. Concr. Compos. (2016). doi:10.1016/j.cemconcomp.2016.11.006.

799 [40] S. Jacobsen, J. Marchand, H. Hornain, Sem observations of the microstructure of frost
800 deteriorated and self-healed concretes, Cem. Concr. Res. 25 (1995) 1781–1790.
801 doi:10.1016/0008-8846(95)00174-3.

802 [41] C. Edvardsen, Water permeability and autogenous healing of cracks in concrete, ACI
803 Mater. J. 96-M56 (1999) 448–454.

804 [42] L. Ebensperger, R. Torrent, Concrete air permeability “in situ” test: status quo, Rev.
805 Ing. Construcción. 25 (2011) 371–382.

806 [43] M. Aguayo, S. Das, A. Maroli, N. Kabay, J.C.E. Mertens, S.D. Rajan, G. Sant, N. Chawla,
807 N. Neithalath, The influence of microencapsulated phase change material (PCM) characteristics
808 on the microstructure and strength of cementitious composites: Experiments and finite

809 element simulations, Cem. Concr. Compos. 73 (2016) 29–41.
810 doi:10.1016/j.cemconcomp.2016.06.018.
811